# VALIDATION OF ARTEMIS I AEROTHERMAL DESIGN MODELS USING DEVELOPMENTAL FLIGHT INSTRUMENTATION

**Brandon L. Mobley**
NASA Marshall Space Flight Center, Aerothermodynamics Team Lead, Huntsville, Alabama

**Samantha Summers, PE**
NASA Marshall Space Flight Center, GeoControl Systems, Huntsville, AL

## ABSTRACT

The inaugural flight of the Space Launch System (SLS) Block 1 launch vehicle, Artemis I, occurred on November 16, 2022, and featured a full suite of Developmental Flight Instrumentation (DFI) that provided aerothermodynamic measurements to assess thermal design and substantiate aerothermodynamic models. The Block 1 launch vehicle aerothermal instrumentation consisted of approximately 277 aerothermal gauges mounted throughout the Orion Multi-Purpose Crew Vehicle (MPCV), Integrated Spacecraft and Payload Element (ISPE), Core Stage (CS) and Solid Rocket Boosters (SRB) and an additional 179 thermal gauges on the Orion Crew Module (CM). Instrumentation included calorimeters, radiometers, pressure transducers, gas temperature probes, and thermocouples. Data was collected from lift-off through CS Main Engine Cut-Off (MECO). The flight data was invaluable for determining aerothermal model performance and developing flight-derived aerothermal environments for flight reconstruction thermal analysis and future SLS aerothermal models. The data offered critical insights into the aerothermodynamic conditions experienced during the launch and ascent of the SLS vehicle. This study compares the flight-derived environments to pre-existing design models. The aerothermal models were constructed using MINIVER[1], the aerothermal engineering code which predicts aerodynamic heating and acts as an integration tool for incorporating databases from computational fluid dynamics (CFD) simulations and wind tunnel test data. The comparisons reveal the fidelity of the design models, highlighting areas where the design models accurately predicted flight conditions and instances where deviations were observed. Preliminary results suggest that while the design models largely aligned with the observed flight data, there were unique observations that reflected needed areas of model refinement. Aerothermal flight data from Artemis I for the SLS Block 1 vehicle will be further utilized to enhance the accuracy of Block 1B and Block 2 aerothermal models, ensuring improved safety and performance for subsequent Artemis missions.

*Notice to the Reader*

*The Space Launch System, including its performance and certain other features and characteristics, have been defined by the U.S. Government to be Controlled Unclassified Information (CUI). Information deemed to be CUI requires special protection and may not be disclosed to an international audience. To comply with CUI restrictions, details such as absolute values have been removed from plots and figures. It is the opinion of the authors that, despite these alterations, there is no loss of meaningful technical content. Analytical methodologies and capabilities are discussed, technical results and trends are presented, conclusions are captured.*

## NOMENCLATURE, ACRONYMS, ABBREVIATIONS

| | |
|---|---|
| BET | Best Estimated Trajectory |
| BHS | Base Heat Shield |
| BSM | Booster Separation Motor |
| CAD | Computer-Aided Design |
| CAPU | Core Auxiliary Power Unit |
| CEC | Chemical Equilibrium Code |
| CFD | Computational Fluid Dynamics |
| CM | Crew Module |
| CS | Core Stage |
| CUBRC | Calspan University of Buffalo Research Center |
| DAU | Data Acquisition Unit |
| DFI | Developmental Flight Instrumentation |
| DOL | Day of Launch |
| EMHS | Engine Mounted Heat Shield |
| FOV | Field of View |
| GN&C | Guidance, Navigation & Control |
| GRAD | Gaseous Radiation |
| GTP | Gas Temperature Probe |
| ICPS | Interim Cryogenic Propulsion Stage |
| ISPE | Integrated Spacecraft and Payload Element |
| JM | Jettison Motor |
| LAS | Launch Abort System |
| LH2 | Liquid Hydrogen |
| LO2 | Liquid Oxygen |
| LVSA | Launch Vehicle Stage Adapter |
| M | Mach |
| MECO | Main Engine Cut Off |
| MFOV | Medium Field of View |
| MPCV | Multi-Purpose Crew Vehicle |
| MSA | MPCV Spacecraft Adaptor |
| MUF | Model Uncertainty Factor |
| OML | Outer Mold Line |
| PGR | Post Green Run |
| PIFS | Plume-Induced Flow Separation |
| Re | Reynolds Number |
| RMC | Reverse Monte Carlo |
| SAJ | Spacecraft Adapter Jettisoned |
| SLS | Space Launch System |
| SRB | Solid Rocket Booster |
| SM | Service Module |
| SPF-3 | Standardized Plume Field 3 |
| TMM | Thermal Mismatch |
| TPS | Thermal Protection System |
| WFOV | Wide Field of View |

## INTRODUCTION

While the Apollo program ended NASA's campaign to put man on the moon nearly 50 years ago, the Artemis program marked NASA's official return to lunar exploration. Artemis I was an uncrewed Moon orbiting mission that completed a total of 25 days in space, with its main objective to test the integrated vehicle and the Orion spacecraft performance in preparation for subsequent Artemis missions including crew. These missions seek to reestablish a human presence on the Moon and develop further capabilities for Mars exploration.

Artemis I was the first integrated flight of the Block 1 vehicle that combined the Orion spacecraft with the Space Launch System (SLS) rocket. The Orion Multi-Purpose Crew Vehicle (MPCV) consists of a Launch Abort System (LAS), Spacecraft Adapter Jettisoned (SAJ) Panels, Crew Module (CM), and Service Module (SM). The Orion MPCV is connected to the SLS vehicle by means of the Integrated Spacecraft and Payload Element (ISPE). The ISPE is comprised of the MPCV Spacecraft Adaptor (MSA), an Interim Cryogenic Propulsion Stage (ICPS), and the Launch Vehicle Stage Adapter (LVSA). The LVSA attaches to the Core Stage (CS) which contains both the Liquid Oxygen (LO2) and Liquid Hydrogen (LH2) propellant tanks. For its propulsion, the CS has four RS-25 LH2/LO2 Engines. Connected to either side of the CS are two five-segment solid rocket boosters (SRBs). Both the RS-25 CS Engines and the four-segment SRBs were existing hardware developed under the Space Shuttle Program. The five-segment SRB was developed under Constellation. An expanded view of the Block 1 vehicle is shown in Figure 1.

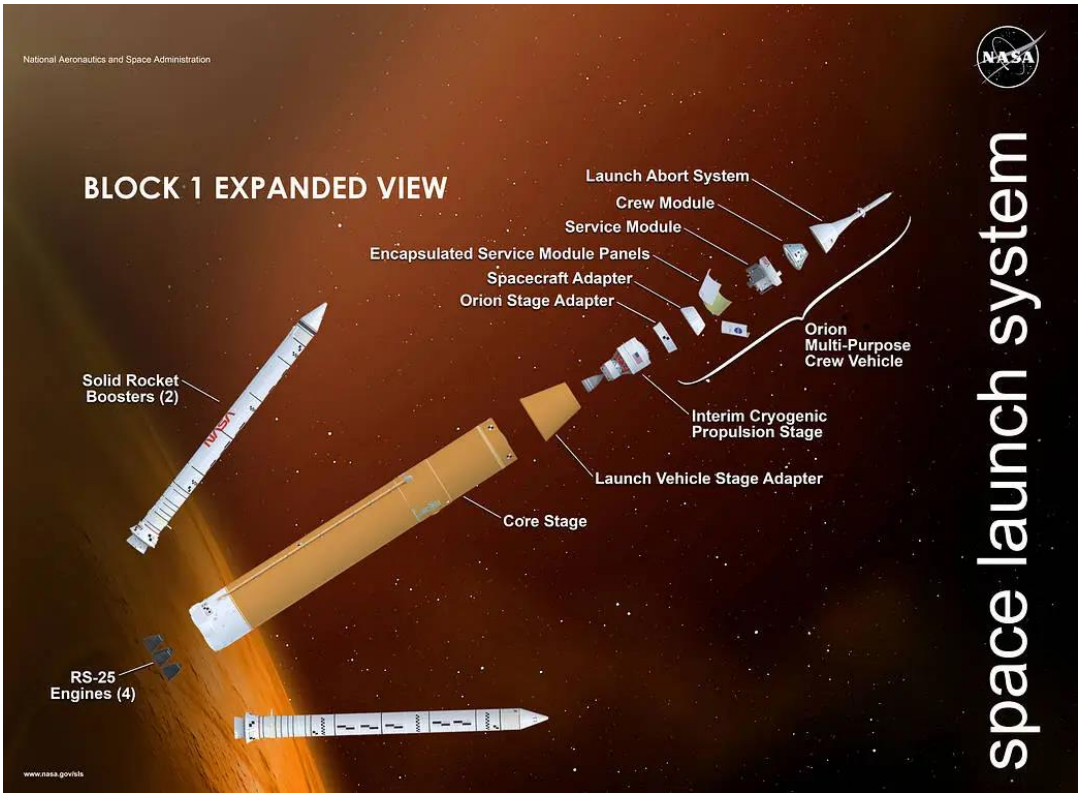


**Figure 1. Expanded view of the SLS Block I vehicle configuration.[2]**

The Aerosciences Branch at NASA Marshall Space Flight Center had the responsibility to develop aerothermal environments for the ascent portion of the Artemis I mission. Ascent was defined as lift-off to CS Main Engine Cut-Off (MECO), covering roughly eight and a half minutes as the vehicle left Earth and flew through the densest parts of the atmosphere on its way to orbital insertion. Several major flight events that impacted the aerothermal environments include maximum dynamic pressure, SRB separation, LAS jettison, SAJ panel separation, and finally CS MECO. Figure 2 depicts the timing of such events for the ascent portion of the Artemis I mission.

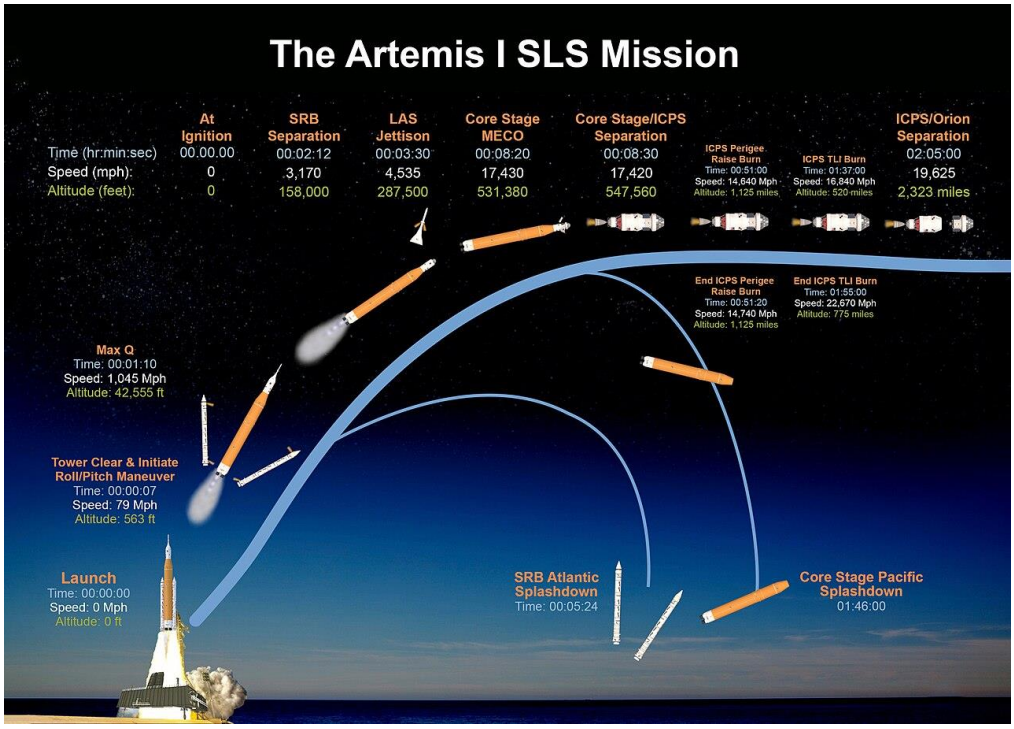


**Figure 2. Artemis I ascent mission timing.[2]**

The purpose of this paper is to provide an overview of the aerothermal measurements collected during the Artemis I launch and to compare the flight data against the methodologies that went into developing aerothermal models and design environments. The analysis stripped the models of any conservatism, which allowed model predictions to be directly compared to flight data. Given the extent of flight data, a summary of the overall model performance is presented, conclusions and lessons learned follow.

## DEVELOPMENTAL FLIGHT INSTRUMENTATION

Aerothermal Developmental Flight Instrumentation (DFI) was installed throughout the launch vehicle elements to capture the aerodynamic heating and plume phenomena that were either direct measurements of heat transfer (convection, radiation) or characterized fundamental fluid dynamics (pressure, temperature) that were drivers to the heat transfer at the surface of the vehicle. Aerothermal gauges were installed at acreage areas or on protuberances as close to design locations where predictions were available and provided substantiating data to the models that were leading drivers to the thermal design.

Coordinated groupings of instruments at selected locations lead to complete characterization of the heating environments to maximize flow field understanding and SLS Block 1 mathematical model validation. The groupings generally consisted of an “island-type” thermal isolator whereby a Schmidt-Boelter calorimeter (with a thermocouple embedded at the thermopile to capture the relative gauge temperature) was mounted, co-located with a static pressure transducer as shown in Figure 3. In the launch vehicle base regions, radiometers and gas temperature probes (GTPs) were also utilized in the groupings to capture additional plume characteristics, shown in Figure 4. Aerothermal DFI generally was sampled at 50Hz, with exception of multi-disciplinary pressure transducers whereby the sample frequencies were significantly increased to accommodate aeroacoustics. On Orion MPCV, there were a total of 22 DFI groupings that contained a pressure sensor, calorimeter, and thermocouple measurement. There were an additional 176 thermal gauges on the CM that were used to estimate heat flux post LAS Jettison and during entry. The DFI on the ISPE was only installed on the LVSA portion of the ISPE and consisted of three groupings each containing a pressure sensor, a calorimeter, and a thermocouple measurement. The DFI on the CS consisted of 38 locations containing a total of 27 pressure sensors, 38 calorimeters, 38 thermocouple measurements, 8 radiometers, and 7 GTPs. The DFI on the CS Engines consisted of 5 groupings containing a total of 3 pressure sensors, 5 calorimeters, 5 thermocouple measurements, 3 radiometers, and 2 GTPs. The DFI on the SRBs consisted of 25 groupings containing a total of 23 pressure sensors, 24 calorimeters, 24 thermocouple measurements, 4 radiometers, and 2 GTPs.

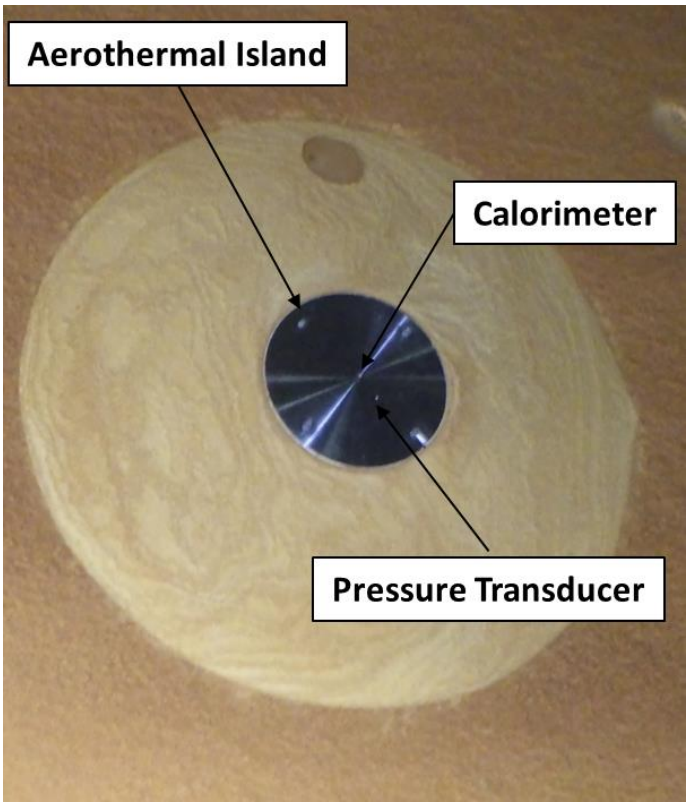


**Figure 3. Aerodynamic DFI grouping consisted of a calorimeter/thermocouple pair and a static pressure transducer.**

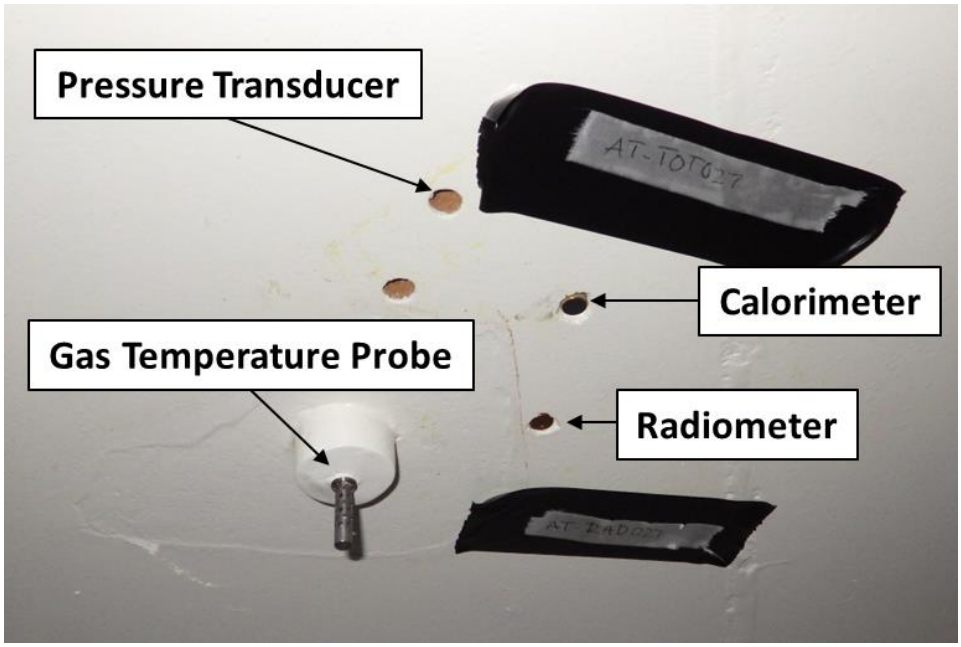


**Figure 4. DFI in the base region include radiometers and GTPs.**

## FLIGHT DATA ADJUSTMENTS

Gauge data was adjusted for discrepancies that were observed in both pre-flight and post-flight operations. Pre-flight, off-nominal, gauge outputs occurred during ground test check-outs, which included pressure, temperature bias errors and continuity issues between the gauge and Data Acquisition Unit (DAU). Pre-flight gauge inspection photos and laser scans were used to capture the as-built Outer Mold Line (OML) discrepancies from that of the Computer-Aided Design (CAD) based model. Ground imagery from the pad and flight imagery from the vehicle cameras and remote launch support systems were utilized to capture transient changes in local vehicle boundary conditions affecting gauge responses. This included ice formation, Thermal Protection System (TPS) offgas and char formation, and transient plume phenomena. Combined with discrete flight events, ground visual data, IR, and flight imagery were all used to adjust and synchronize the post DAU gauge signals with the Best Equivalent Trajectory (BET), examples are as follows.

Prior to lift-off and during tanking operations, the formation of frost or ice occurred on the exterior sensor islands located on the cryogenic portions of the vehicle. Imagery of tanking events showed that frost or ice formed on the surface of some aerothermal sensors that were located on SLS LOX and LH2 tanks and the adjacent structures. Assessment of the flight data at these locations showed unsteady heating values early in flight. This flight regime was normally characterized by aero-cooling conditions. The variation in induced heat transfer to the thermopile due to the icing conditions appeared to dissipate prior to Mach 1 transition; afterwards, the removal or melting of the ice resulted in heating measurements that were in-family with other gauges and pre-fight models, making the signal acceptable throughout the rest of the flight. Figure 5 provides an example of a DFI sensor on the CS LOX tank that was impacted by frost build up. Collective observations from gauges revealed that the icing conditions did in fact dissipate and the data therefore was incorporated into post flight analyses.

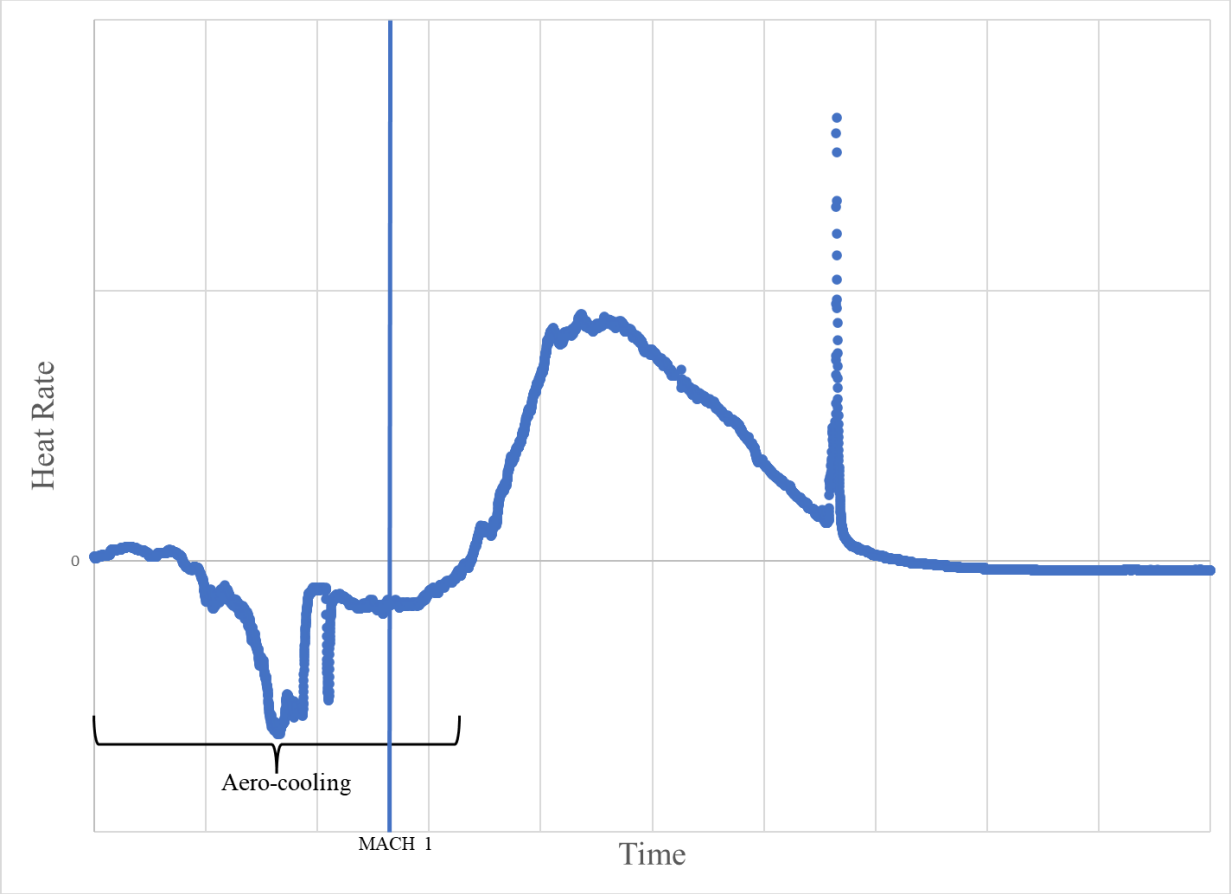


**Figure 5. CS calorimeter that had frost build up on the sensor, later determined to be usable.**

On board data filtering of gauges imposed some unique repercussions to the post processed data. The on-board Data Acquisition System sampled the calorimeter measurements with a signal conditioning card that incorporated both a digital Finite Impulse Response and Infinite Impulse Response filter capability. Use of the data filter caused two problems with the raw calorimeter and radiometer heat flux data. First, the filter induced a delay to the calorimeter response depending on the specific filter used. While as expected, the calorimeter thermopile response time was larger than the local thermocouple response time, the delay in heating relative to the rise in temperature lead to a clear mismatch with the observed physics in the induced event. Using the master event timeline, the data was post-processed to optimize offset corrections from all calorimeter and radiometer data. Figure 6 shows an example of the observed lag in the calorimeter data in comparison to the corresponding thermocouple data. The second filter-induced problem resulted in the potential reduction in the transient, peak heat flux due to the usage of the filter at the 50Hz sample frequency. Short duration peaks were not recorded accurately because the filter fundamentally imposed a time-average of the data. There were no corrections, or thermal issues associated from the characteristics due to this issue, but there may be impacts to the accuracy of the magnitudes and duration of short peak heating events. Figure 6 is also an example of one of these short peak heating events where the magnitude and durations may have been clipped due to filtering.

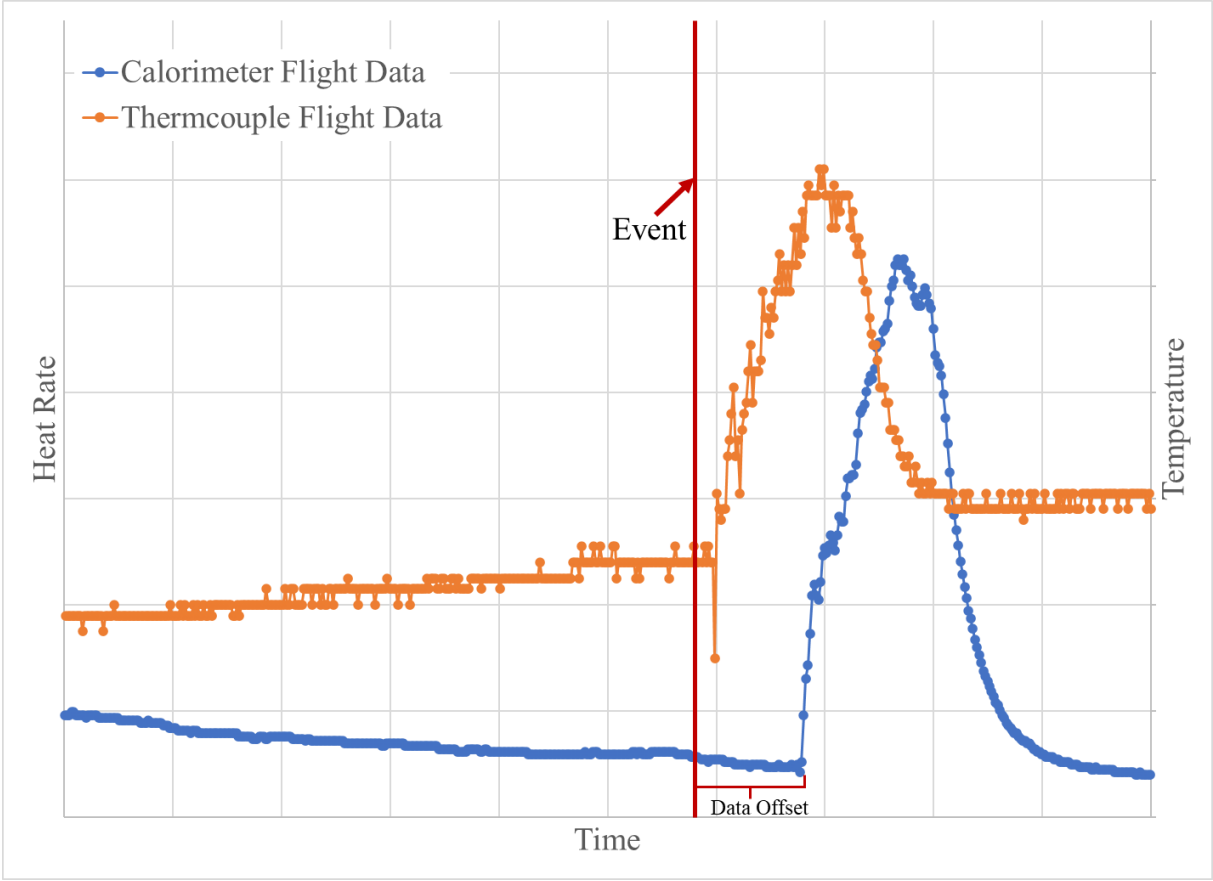


**Figure 6. Artemis I calorimeter data shows a filtering induced offset.**

A calorimeter response is the result from the total heat balance at the sensor and is often paired with the output from a thermocouple located at the thermopile to record the relative gauge temperature. Included in this balance is the energy re-radiated from the surface of the sensor. Artemis I was instrumented using Schmidt-Boelter type calorimeters that utilize a copper heat sink to keep the local thermopile at a reference temperature, within the operational range, which also serves to keep the gauge cool, thereby minimizing the re-radiation from the sensor surface. Depending on the relative wall temperature and driving thermal potential, the re-radiation flux is typically assumed to be negligible with respect to the induced heat flux. However, at very low heating conditions when calorimeter surface re-radiation and aeroheating are similar in magnitude, this assumption is no longer valid. Due to low density flow at high altitudes, the induced convective heating is low, whereby calorimeters may reflect negative heating. Adjustments were made to the calorimeter measurements to include re-radiation in the energy balance and were generally applied to signal responses following SRB separation, during the rarefied flow regime. Although the adjustments were small, the adjustment resulted in excellent agreement with theoretical high altitude, low magnitude, rarefied flow and free molecular flow heating rates. Figure 7 is an example of the re-radiation adjustment made to the flight data.

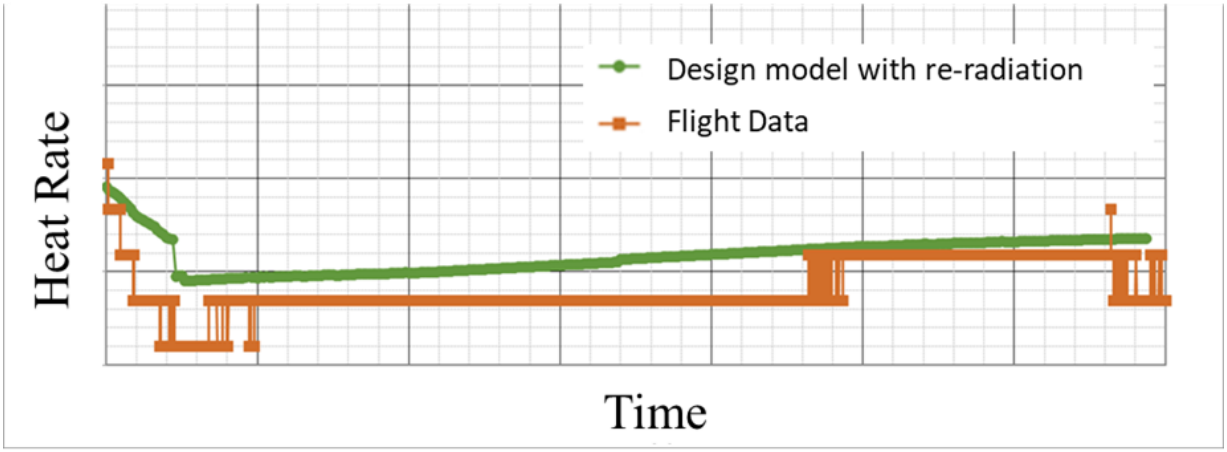


**Figure 7. Artemis I flight data with calorimeter surface re-radiation effects.**

When a relatively cold calorimeter is surrounded by higher temperature insulating TPS materials, this produces a sharp discontinuity of the thermal boundary layer which can lead to measurement error of the convective flux environment. When flow passes over a temperature discontinuity (i.e. a cold sensor in a hot wall), the temperature gradient in the boundary layer must change drastically in order for the temperature profile to remain continuous. Since the thermal gradient of the gas at the wall is the driving potential towards heat transfer, it too changes abruptly at the temperature jump. This boundary layer problem has historically been known as Thermal Mismatch (TMM). Uncorrected island measurements for Shuttle were found to have errors as large as 100% or more in peak heating regions. The method of Westkaemper[3] has been utilized to make TMM corrections to the calorimeter measurements for all DFI groupings that include TPS surfaces immediately upstream of the DFI Island. Iteratively, a thermal model was used in conjunction with the heat rate data to determine the TPS surface temperature forward of the DFI island. This methodology was not implemented on protuberances or in non-aerodynamic heating regions. Figure 8 is an example of the reduced hot wall heating rates resulting from TMM corrections. In this example the peak measured heating rate had a 35% reduction.

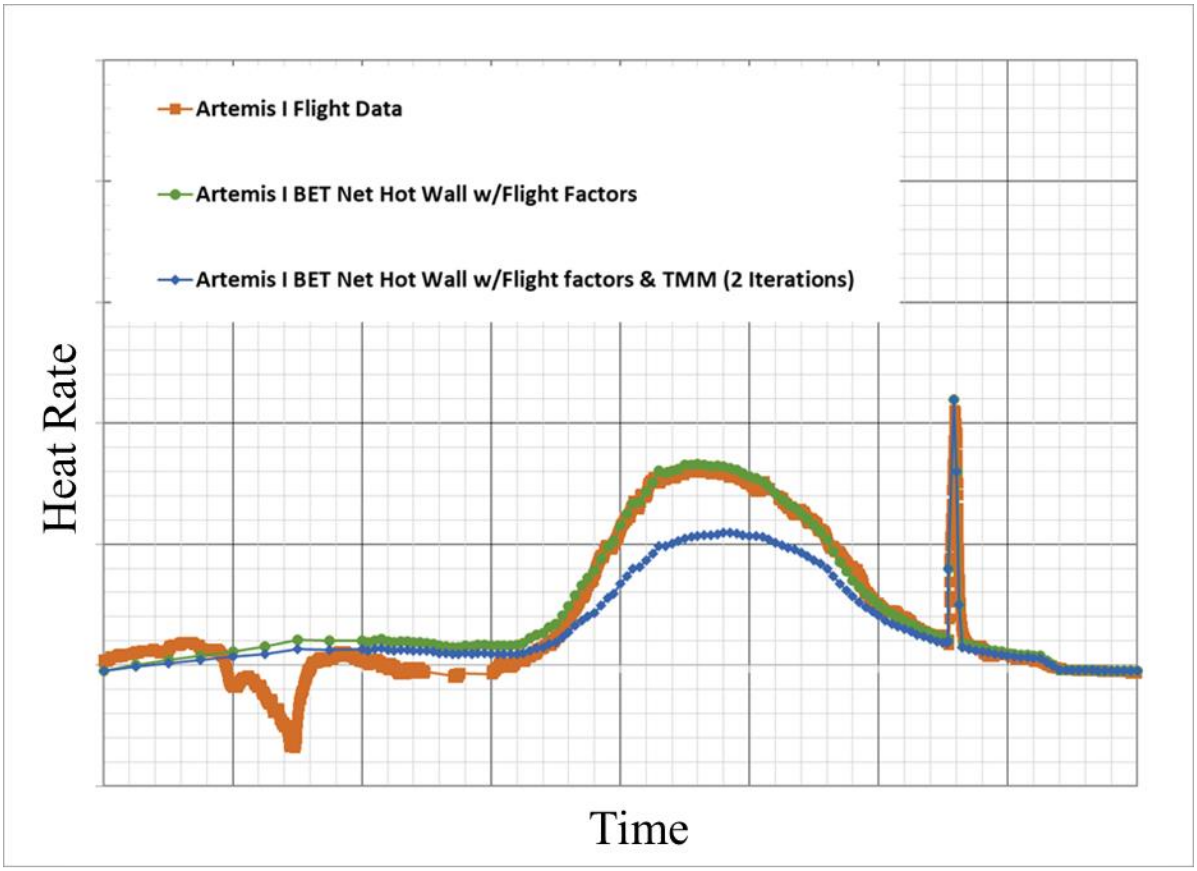


**Figure 8. Reduced hot wall heating rates due to thermal mismatch correction.**

Wide field-of-view (WFOV, 150 degrees, full angle) and medium field-of-view (MFOV, 79 degrees, full angle) radiometers were flown for the purposes of determining plume-induced radiation and backing-out convection from the total heat flux captured by calorimeters. The radiometers utilized a sapphire window to block convective heating, the measured integrated incident radiation covering a wavelength range from approximately 0.4-5 microns at an average 0.85 transmittance, with the transmittance tail-off extending to approximately 7 microns. There were fifteen radiometers flown on Artemis I that were subject to radiation from the SRB and RS-25 exhaust plumes. During flight, the windows on these radiometers were not purged with gaseous nitrogen and were subject to surface contamination from TPS offgas, smoke, carbon soot and aluminum-oxide particles in the immediate vicinity of the gauges. From lift-off to SRB separation the TPS offgas attenuated the plume radiation leading to a reduction in the radiative heat flux in comparison to the pre-flight predictions. Attenuation of the plume radiation due to offgas was observed specifically in aft-facing radiometer responses. Broadside viewing radiometers appeared to be less affected and in better agreement with pre-fight predictions. The radiometer installation on the core stage base areas resulted in approximately a ±1 degree uncertainty of the bore sight vector. The RS-25 MFOV radiometers were installed with a larger ±5 degree tolerance which resulted in a greater uncertainty of the radiometer bore sight vector. Uncertainty of the MFOV radiometer bore sight vector resulted in potential variation in view factor of the plume, and subsequent uncertainty in determining the convective heat flux. In backing-out local convection at

the RS-25 nozzle, due to the reduced field of view (FOV) of the radiometers, radiative heat flux adjustments were made to correct the scaled output (radiometer outputs were calibrated using a full FOV reference calorimeter). Flight radiation data was used, however the stack-up of adjustments and uncertainty in view factor were considered when estimating the range of convection experienced during flight. An example of radiometer adjustments can be seen in Figure 9.

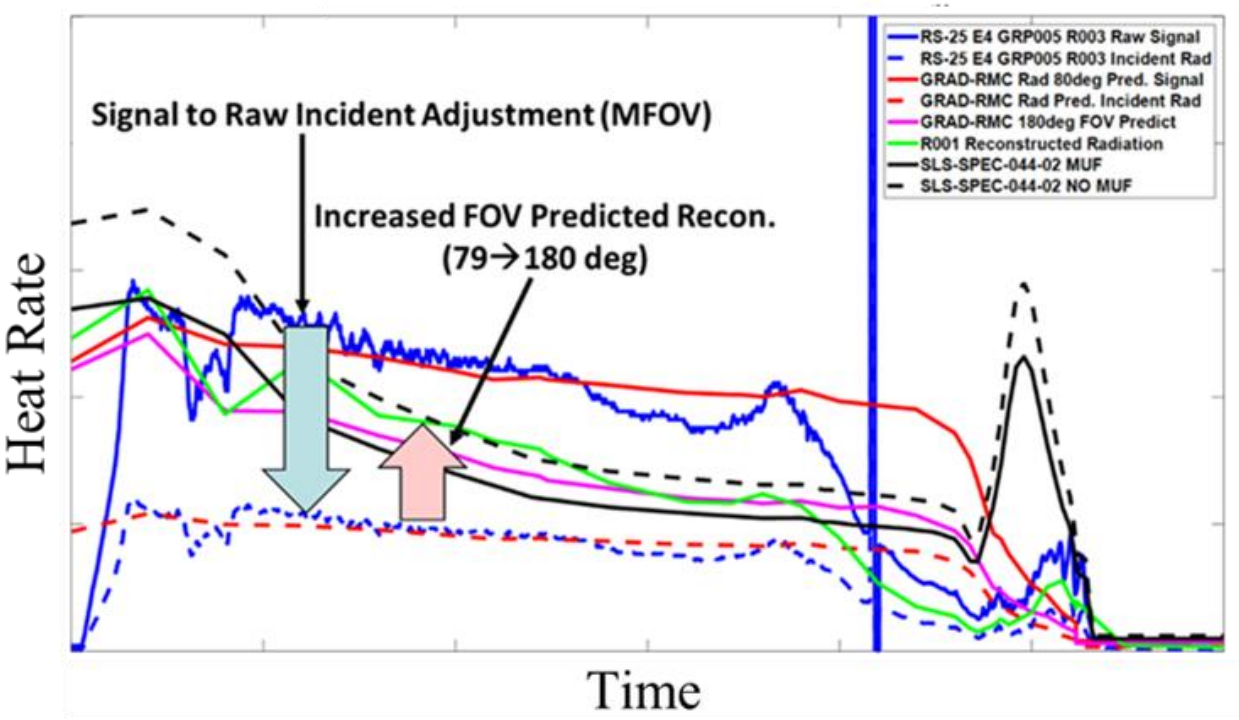


**Figure 9. RS-25 MFOV radiometer response and adjustment outputs for determining plume-induced convection.**

## VALIDATION OF AEROTHERMAL DESIGN MODELS

The SLS Block 1 aerothermal design environments developed for Artemis I were the result of discrete spatial models (known as body point models) that fully integrate aerodynamic and plume-induced heating predictions which were a function of the vehicle geometry, trajectory, propulsion system characteristics and local TPS conditions. Plume-induced environments consist of CS RS-25 and SRB plume base heating, LAS Jettison Motor (JM) plume impingement, Booster Separation Motor (BSM) plume impingement, and Core Auxiliary Power Unit (CAPU) exhaust disposal. Further details about the methodology behind the aerothermal design models can be found in the AIAA paper *Overview of Space Launch System Ascent Aerothermal Environments*[4] which was produced by the Aerosciences Branch. This section provides details on how the DFI data was used to further substantiate and revise each aerothermal model for subsequent SLS Block 1, Block 1B and Block 2 missions. The aerothermal design models were evaluated using the actual day of launch input parameters including the BET to develop Artemis I reconstructed aerothermal environments. The expected heating profiles were compared with flight data, the variances were evaluated, and the models, tools, and methodologies were updated as needed.

Aerodynamic Heating

Aerodynamic heating was the largest spatial driver for the aerothermal environments on the SLS vehicle forward of the base engine section. Of the 93 DFI groupings, 60 are considered aerodynamic specific regions.

To compare flight data fairly with the model predicted environments, the design models were evaluated with the flight specific inputs. This involved using flight DFI temperatures to create hot wall model predictions. The model predictions removed all Model Uncertainty Factors (MUF) and used the BET determined by Guidance, Navigation & Control (GN&C). The outcome was a hot wall model prediction that could be directly compared to flight data. Figure 10 provides an example of a gauge on the CS intertank. The figure shows the cold wall (0°F) design environment, the cold wall design model as-run with the BET, the hot wall design model as-run with the BET, and finally the hot wall flight data. It is noted that the design environment is adequately bounding and when flight parameters are considered, the design model is in good agreement with flight data.

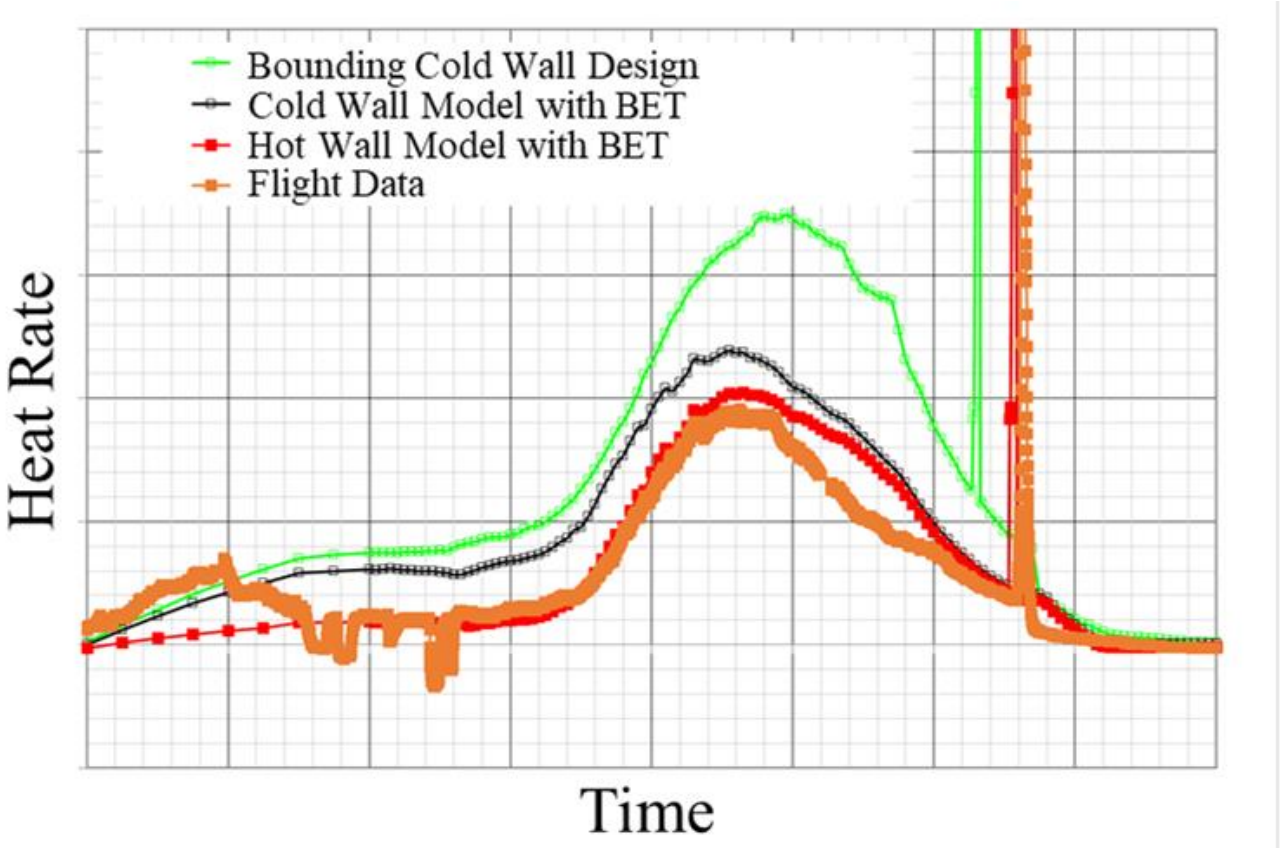


**Figure 10. CS hot wall design environment compared to flight data.**

Aerodynamic heating models accounted for laminar and turbulent heating. Boundary layers transition from laminar to turbulent and vice versa. For an overwhelming majority of the vehicle, the boundary layer quickly goes turbulent, throughout peak heating, and then will transition to laminar at high altitudes. Across the vehicle, flight data showed that the turbulent to laminar transition happened later in flight than what was predicted in design. The transition criteria for the

SLS vehicle was carried over from Constellation and Shuttle which utilized $Re_\Theta/M_\infty$ as the transition parameter. Figure 11 is an example of a gauge on the SRB nose cone where the flight data clearly showed that the boundary layer transition happened later than what was modeled in design. Impacts from implementing a longer duration of turbulent flow would lead to additional heat loading. A flight-derived transition criteria has been implemented across the vehicle.

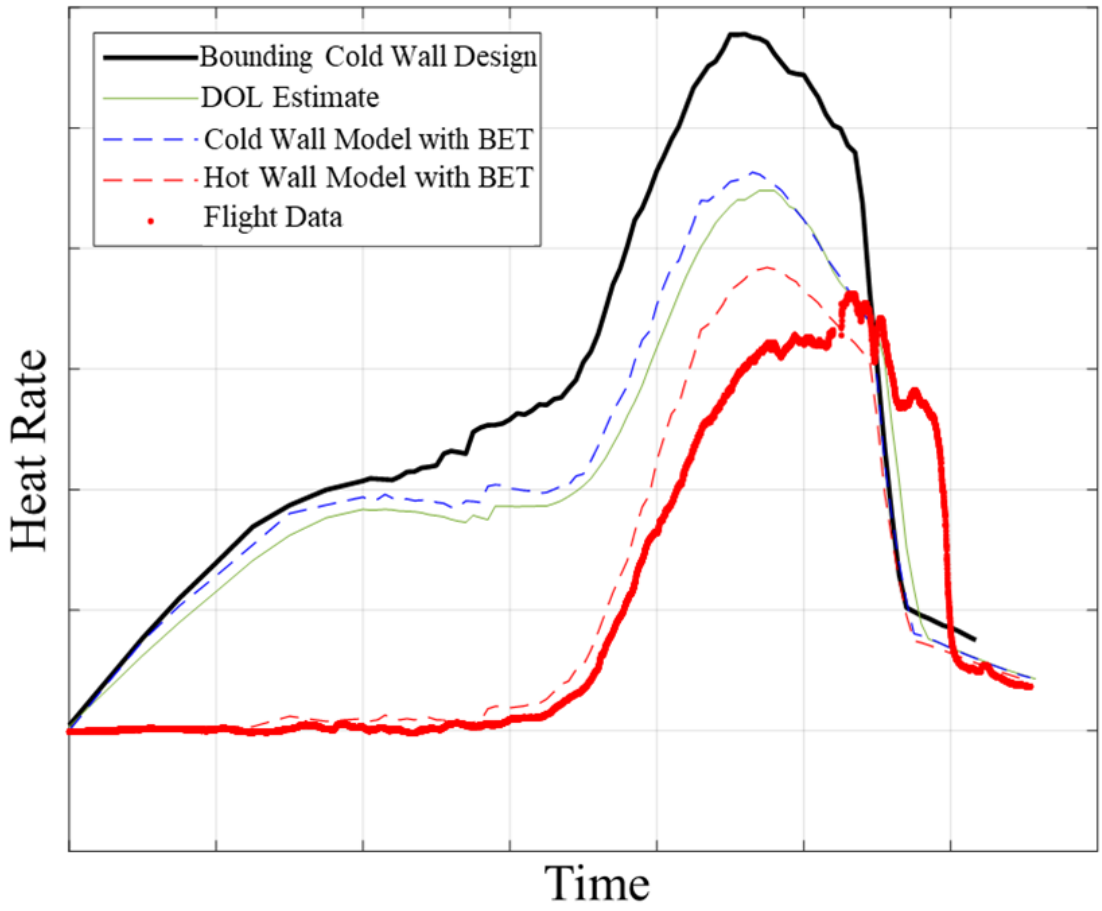


**Figure 11. SRB gauge on the nose cone shows a late boundary layer transition.**

The relative interference between SRB and CS surfaces also affected the local flow boundary layer characteristics in the interactive regions between these vehicle elements. Figure 12 shows an example of a SRB gauge, in front of the forward attach, where no turbulent to laminar transition was observed. One of the biggest observations made from this gauge and all the other gauges located inboard between CS and SRB was that the boundary layer remained turbulent until SRB separation. Similar aerodynamic phenomena occurred in multi-body launch vehicles and aircraft where interference factors are considered; in this case it appeared that the CS and SRB interaction tripped the boundary layer keeping the flow turbulent. Design models inboard between CS and SRB were updated to incorporate this observation.

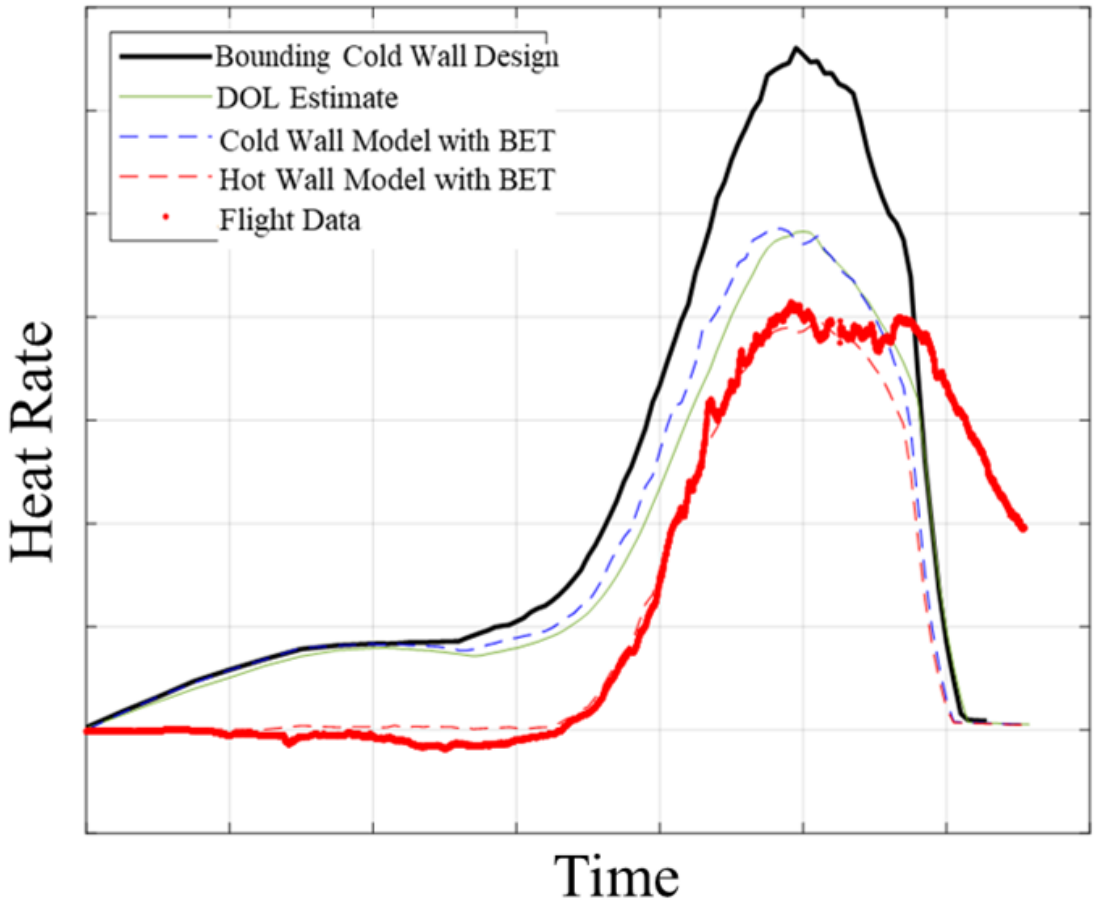


**Figure 12. Inboard SRB gauge where the boundary layer remains turbulent.**

The Aerosciences Branch generated reconstructed flight environments for the entire vehicle. Flight factors were developed to improve models to better agree with flight data. These flight factors were implemented via a Mach Dependent Table. Figure 13 shows the before and after impact of using flight factors to the model previously shown in Figure 10. Additionally, Figure 14 is an example of what the model became after the boundary layer transition was extended and the flight factors were added to the SRB model shown in Figure 11. The flight reconstructed environment matched the flight data relatively well.

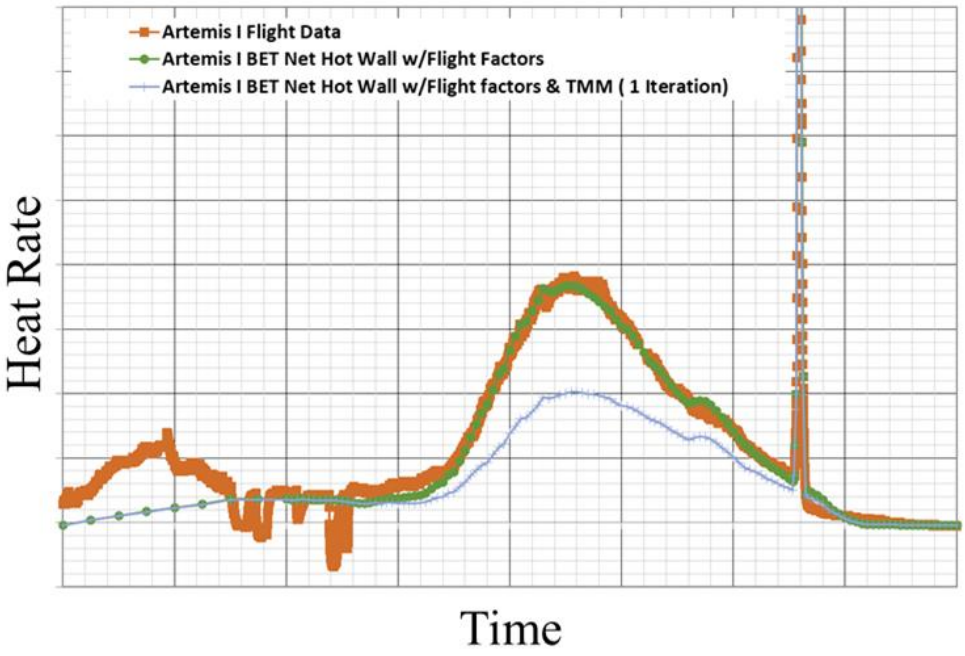


**Figure 13. Flight Factors added to CS design model to create flight reconstructed environments.**

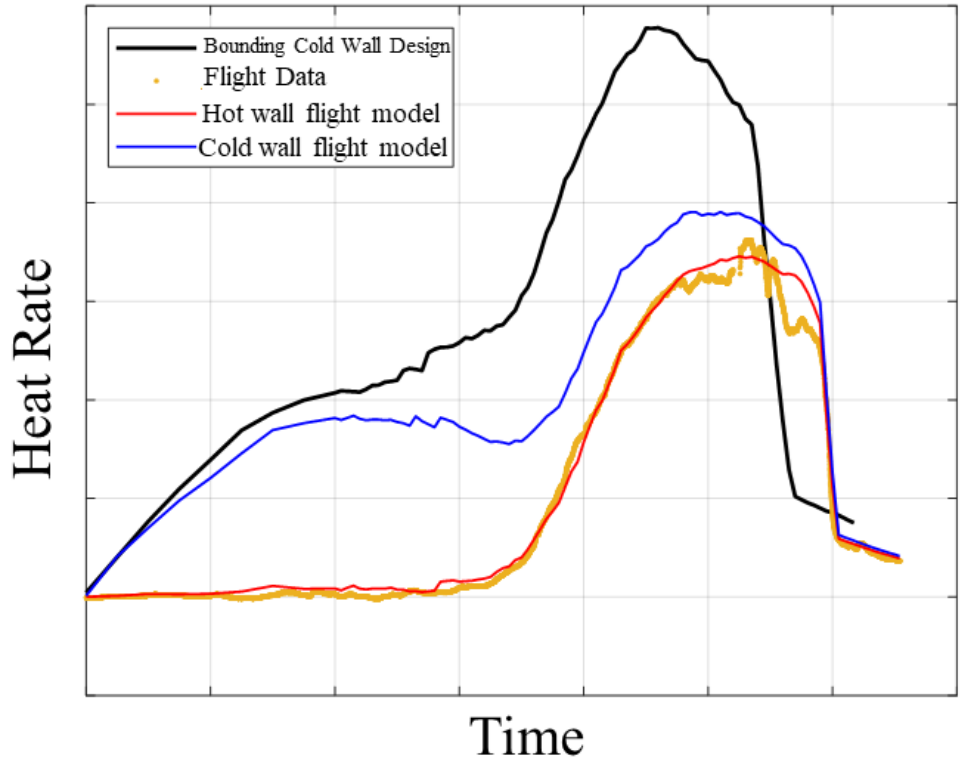


**Figure 14. Flight Factors added to SRB design model to create flight reconstructed environments.**

Thermal Mismatch (TMM) was observed from all calorimeters that were imbedded in TPS. Figure 15 and Figure 16 show the impact of TMM corrections. As shown, the hot wall flight data (not even corrected to cold wall) was higher than the cold wall design environment. Used as-is, the design environment would not be bounding. Once the TMM adjustment was applied to the flight data, the flight heat rate came down significantly. Figure 16 reflects the design environment was conservative.

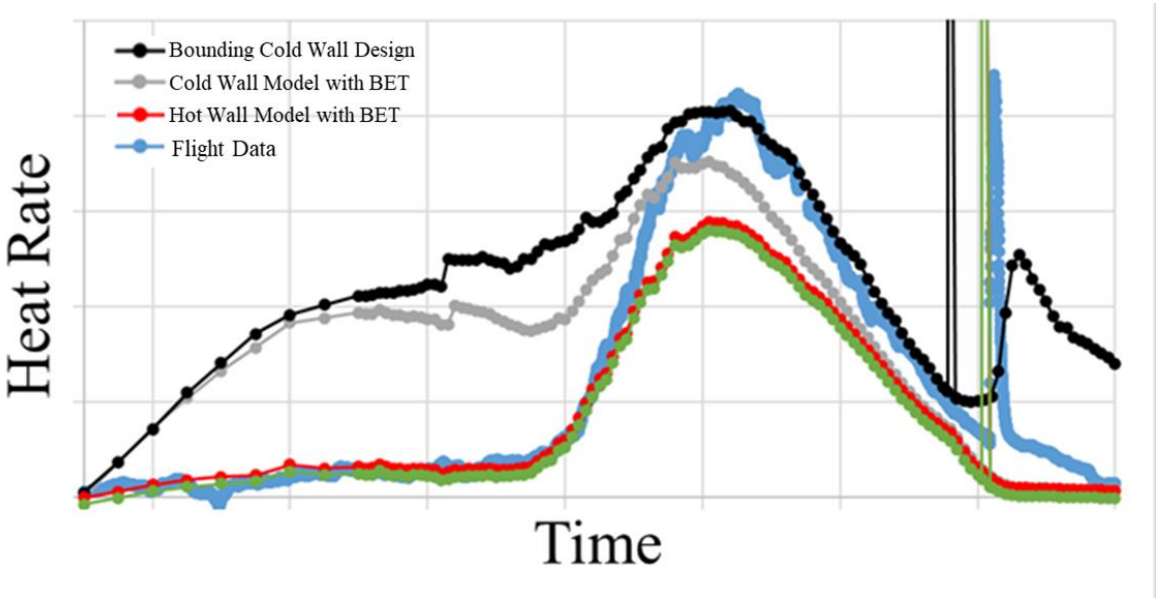


**Figure 15. Without Thermal Mismatch, LVSA has environment exceedances.**

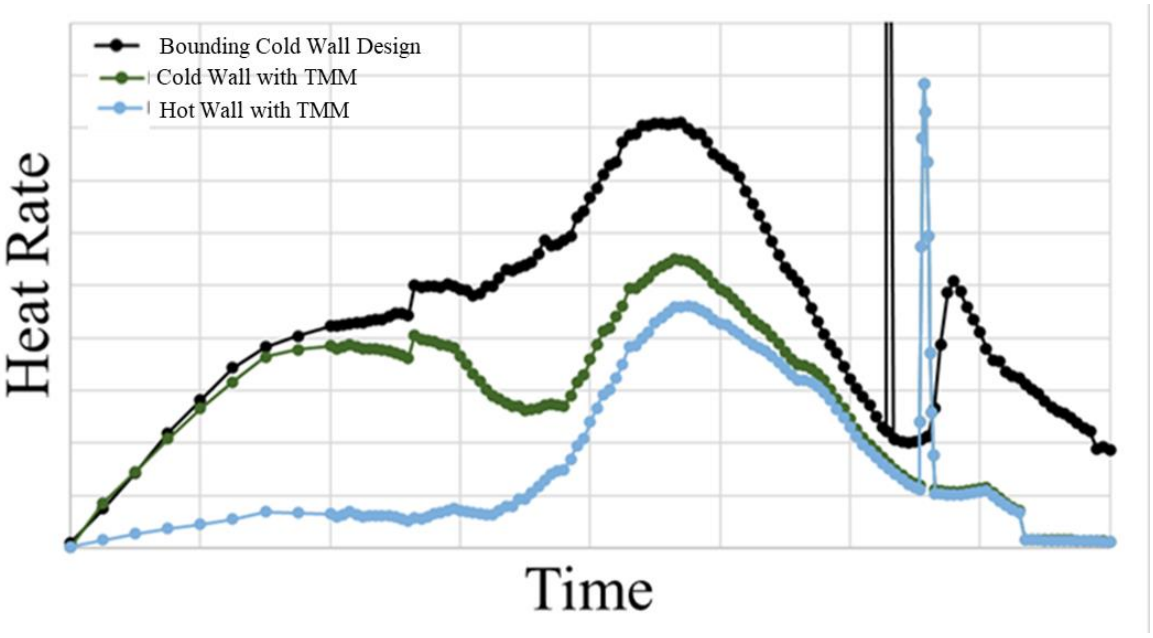


**Figure 16. Thermal Mismatch applied to LVSA minimizes environment exceedances.**

The design models for aerodynamic heating were adequately conservative. Updates to the models were implemented to improve modeling accuracy and reduce conservatism. This included adding flight correction factors to heating, utilizing flight-derived boundary layer transition criteria, and removal of any remaining conservatism from the MUF.

Plume-Induced Radiation

There were fifteen radiometers flown on the Artemis I base to capture the incident radiation from the combined SRB and RS-25 plume flow fields and thermal blackbody surfaces. All the radiometers had a WFOV of 150 degrees except the three RS-25 nozzle radiometers with a MFOV of 79 degrees.

Plume-induced radiation design environments were generated through the development of a radiation database whereby for a given body point the cumulative radiation from the RS-25 and SRB plumes could be interpolated over the altitude, thrust and time space (due to variation in solid rocket motor chamber conditions with time). For SRB plumes, the radiation database utilized maximum SRB chamber conditions found within the design trajectory set dispersions, whereas RS-25 plumes were modeled in accordance with the RS-25 rated power levels. For the purposes of comparing with radiation flight data, plumes were modeled using the flight conditions (i.e. flight trajectory) and radiation predictions were made as a function of altitude. The Chemical Equilibrium Code[5] (CEC) was used to generate the thermodynamic combustion gas database for the nozzle and plume flow fields, RAMP2[6] to predict the nozzle flow fields, and Standardized Plume Field 3[7] (SPF-3) for the plume flow fields. SRB nozzle erosion was accounted for as a function of time. SRB plume gas composition was modeled as 13 species and the aluminum-oxide particles were modeled using five particle bins, the particle sizes ranged from 4 to 9.5 microns. At a discrete altitude, plumes were modeled as single plumes; the combined base flow field including plume-plume interactions, reflected shocks and recirculation was not modeled. Gaseous radiation from the RS-25 plume model was computed using the Gaseous Radiation[8] (GRAD) band model code. The Reverse Monte Carlo[9] (RMC) code was used to predict the radiation from the two-phase solid rocket motor plumes, using a reverse ray trace with 30,000 rays. For a given body point, radiation predictions were made for each RS-25 plume (gas only plume model) and SRB plume (two-phase plume) and then summed to determine the total heat rate. The MUF normally included in design models was not implemented in the flight generated radiation models. The Artemis I derived radiation models were compared to the flight data from the radiometers.

Radiation predictions versus the flight measurements on the CS base heat shield (BHS) are shown in Figure 17. Figure 18 shows a radiation comparison for a gauge on the SRB aft skirt. The predictions exceeded the flight measurements by almost half during the early times in the flight and collapse onto each other for the later portion of flight. Early reduction may be attributed to the cork offgas and combustion products attenuating a significant portion of the incident radiation. Later in flight where flight and BET predictions deviate, overpredictions are attributed to the summing plume radiation approach, as opposed to predicting radiation from the combined interacting plume base flow field. Contamination of radiometer faces was also considered as a contributing factor to the over-predictions of the incident radiative heat flux. Noting the trends

from all the radiation measurements facing aft, a reduction in the design radiation models was warranted.

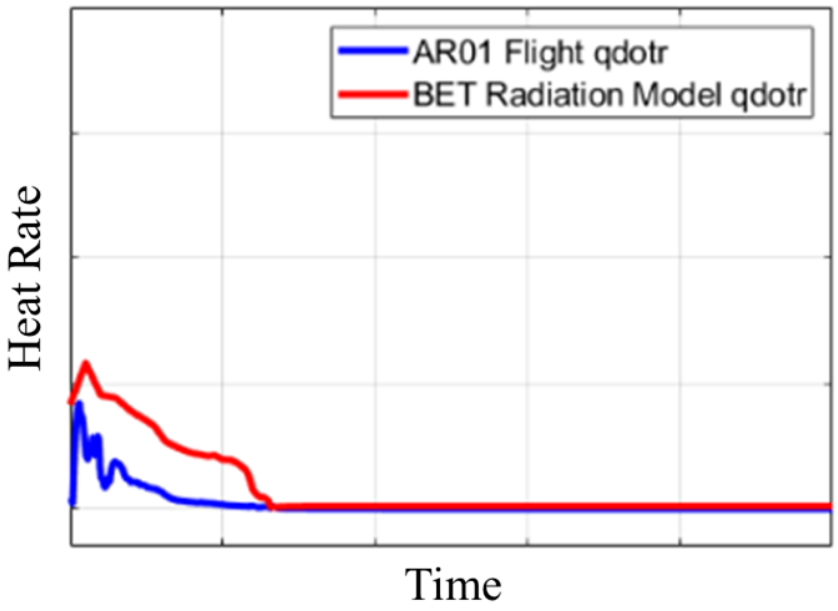


**Figure 17. CS radiation prediction vs radiometer data.**

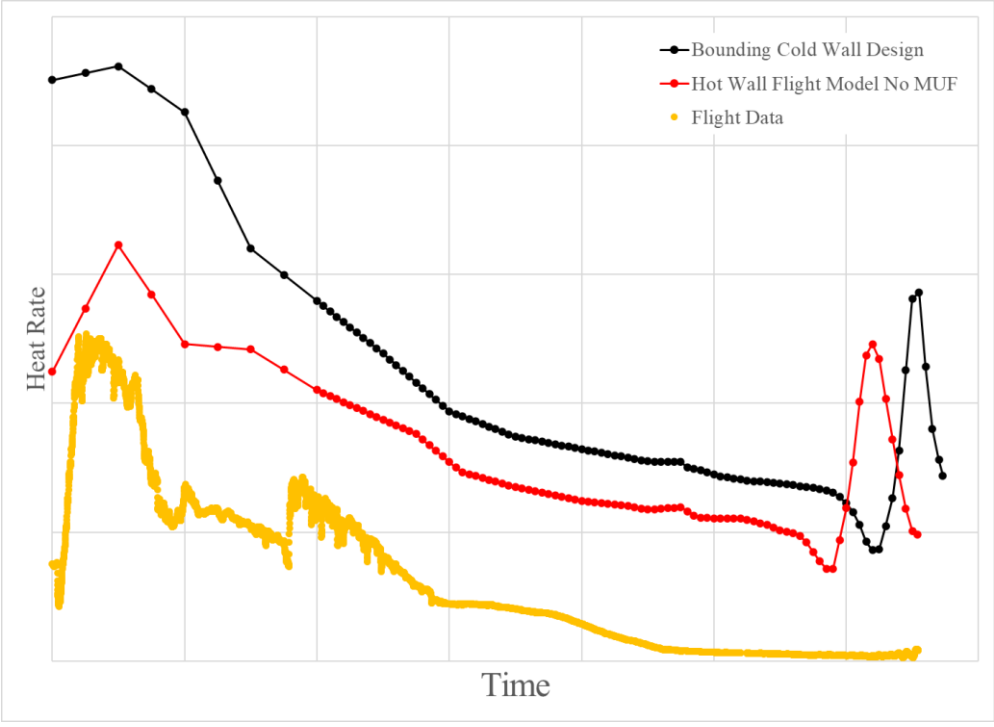


**Figure 18. SRB radiation predictions vs radiometer data.**

As for the radiation on the RS-25 engines, the radiation predictions were all generally conservative and showed good agreement with flight. An example of radiometer flight data with FOV adjustments can be seen Figure 19.

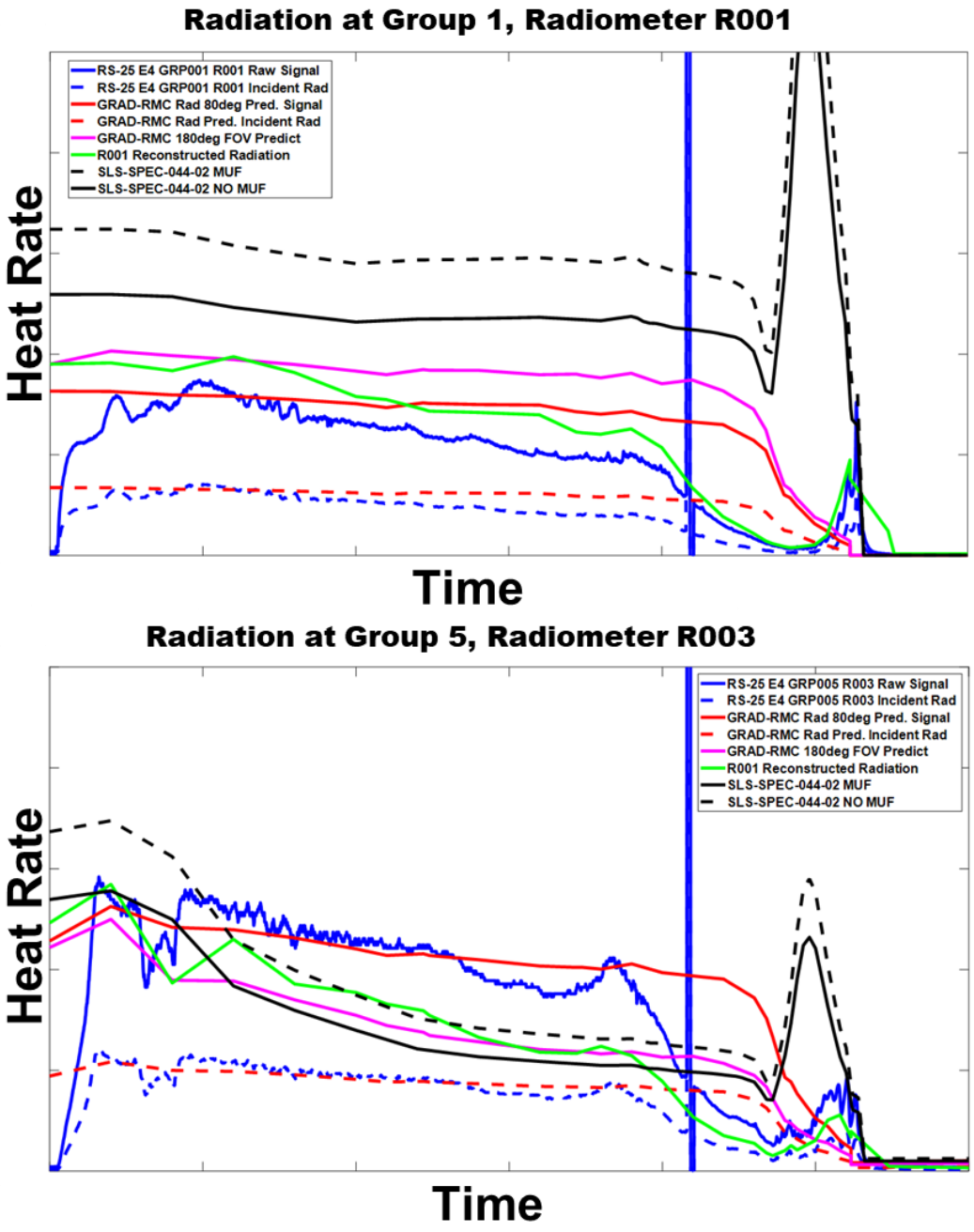


**Figure 19. Artemis I engine external nozzle radiation predictions with flight data.**

Based on comparisons of flight measurements, design, and BET predictions, the MUF was removed, and all aft facing areas received an additional radiation knock down factor. Further investigation of the effects on incident radiation and sensor contamination will be pursued.

Base Plume-Induced Convective Heating

SLS plume-induced base convection design environments were predominantly developed utilizing 2% scale model data from short duration (~40-60ms sample time) hot fire wind tunnel tests performed at the Calspan University of Buffalo Research Center (CUBRC) from 2014-2015. As the SLS CS base design evolved, additional changes to the base design environments were made using CFD models to further account for CAPU exhaust disposal in the base. Artemis I base instrumentation also captured environments during the 2020-2021 Green Run Tests which lead to further observation of CAPU exhaust plume-induced heating and impacts from base TPS offgas and burning. Following the Green Run tests, the design environments were revised to account for the energy release within the base flow field from burning TPS and offgas, increasing convection during the plume-induced aspirating phase of flight until TPS burning was quenched. Post-Green Run (PGR) design environments were developed from ground test data from both full-scale ground tests to redesign BHS TPS prior to delivery of the CS to KSC. Following flight, plume-induced base convection was backed-out using the data from the calorimeters and radiometers, gas temperature probes provided an estimate of the recovery temperature of the recirculated plume gases leading to determination of the local heat transfer film coefficient. A detailed explanation of base heating can be found in the AIAA paper *Space Launch System Base Aerothermodynamics Post-Flight Reconstruction for Artemis I*[10] which was produced by the Aerosciences Branch.

*Core Stage*

Objectively, base flight data was used to substantiate the plume-induced convection models, and furthermore, improve them to account for full scale phenomena that was missed in the scale model tests due to wind tunnel constraints and challenges with SRB plume similitude at 2% scale. Scale model tests were run in shock tunnel and Ludwieg tube modes to best match flight Mach and ambient pressure (plume expansion, shape), the tunnel constrained the tests to a Mach range of 2.8 to 5.2 and altitudes from approximately 50 to 165Kft (higher altitudes were run with no flow up to 211Kft). Figure 20 shows the flow regime transitional characteristics observed in base pressure measurements and reconstructed base convection. Flight data showed the base transition from plume-induced aspiration to recirculating flow occurred lower in altitude than predicted. From flight and CFD analysis it was shown that the recirculation induced by the SRB plume interactions contributed to pressurize the base earlier in flight before the RS-25 plume-plume interactions strengthened. Aside from the additional challenges of modelling the increases in design environments from TPS combustion (from flight data), the composite core stage RS-25 plume interactions with the SRB plumes induced environments were the only other flight regime where the BHS convective design environments increased.

PGR total heat load environments were conservative when compared to post-flight reconstructed environments. Engine shroud and boat tail convective heating profiles showed good agreement in magnitudes and trends with flight environments. There were minor exceedances noted on the boat tail near the SRBs based on flight-derived, reconstructed heating models. Following Green Run, the engine-mounted heat shields (EMHS), or RS-25 nozzle close-out thermal curtains, design environments were not revised to include P50 cork TPS and blanket rain shield burning environments. While there were no gauges directly installed within the RS-25 EMHS, the reconstructed convective environments showed exceedances during the aspiration, TPS burning

phase of flight. Despite areas of exceedances in base convection, the composite, total design heat load bounded the flight environments for all body points in the base. There were no reported base temperature exceedances, or environment-induced anomalies (thermal, or plume-induced, driven failures) for the flight.

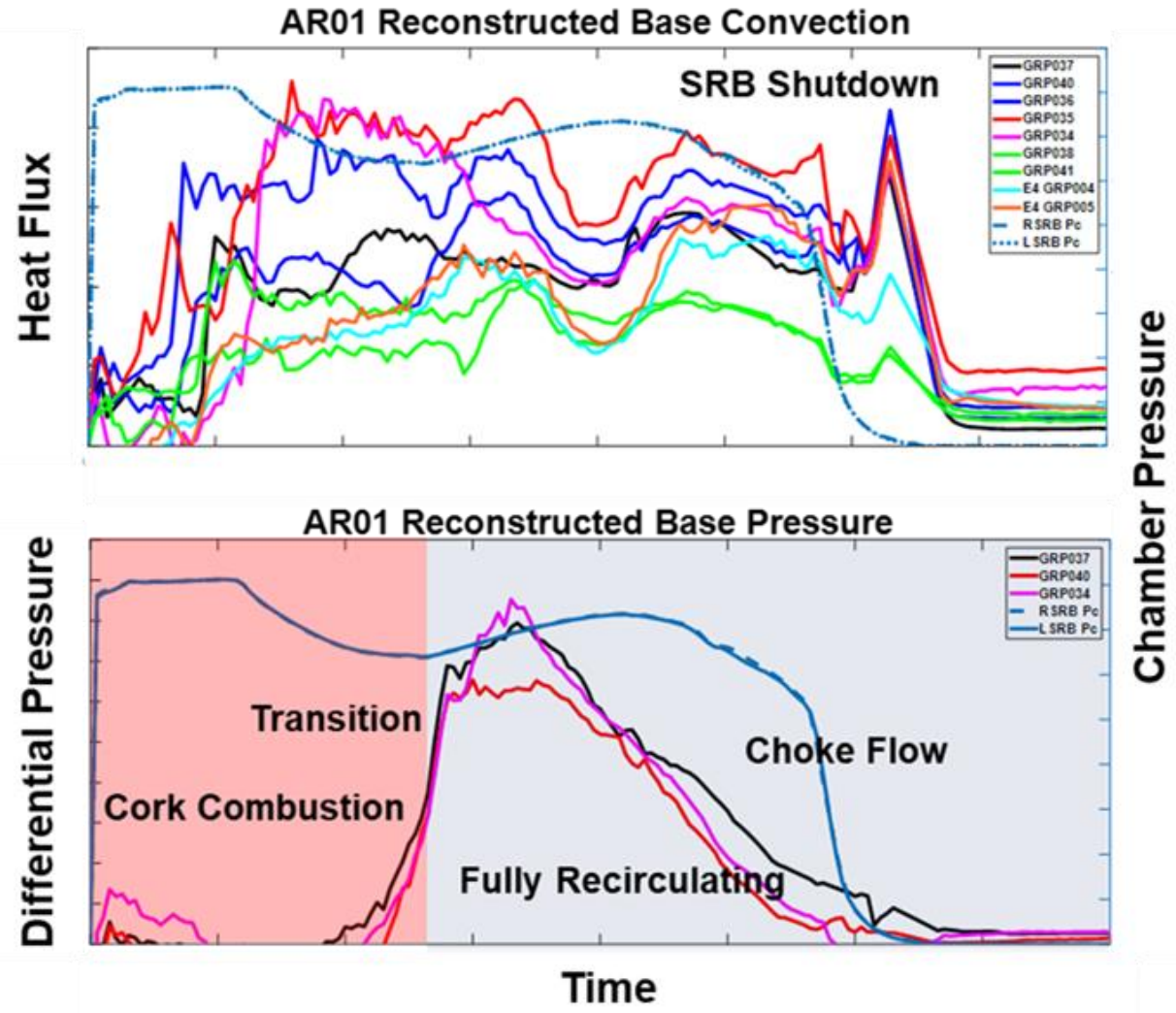


**Figure 20. Artemis I Base Plume-induced Base Convection and Pressure Trends**

The BHS TPS consisted of Hypalon/P50 cork, whereby, given the plume radiation levels, pyrolysis resulted shortly after lift-off. RS-25 and SRB plumes entrained air into the base, the local ignition sources (CAPU free-hydrogen exhaust plumes, hot gas, radiation) impingement on the heat shield which leads to high local convection and RS-25 and SRB plume radiation. During Green Run convective heating environments were observed to be 3x the nominal. The Green Run test campaign provided us with peak energy release due to cork char and pyrolytic gas oxidation. However, this observation was for a static test condition. Since at the time no data was available prior to flight for cork combustion onset or flame-out, PGR models had to make general assumptions. TPS thermal-vac ground tests were performed to characterize the P50 cork offgas and combustion as a function of induced radiation and ambient pressure. Post flight base design

environments were revised, a model was developed to predict the base gas enthalpy following heat release from TPS combustion, over the flight span (lift-off throughout the aspirating flow regime until a quenching condition was met). Figure 21 provides an example of a BHS environment that was updated PGR but the flight data shows the transient characteristic.

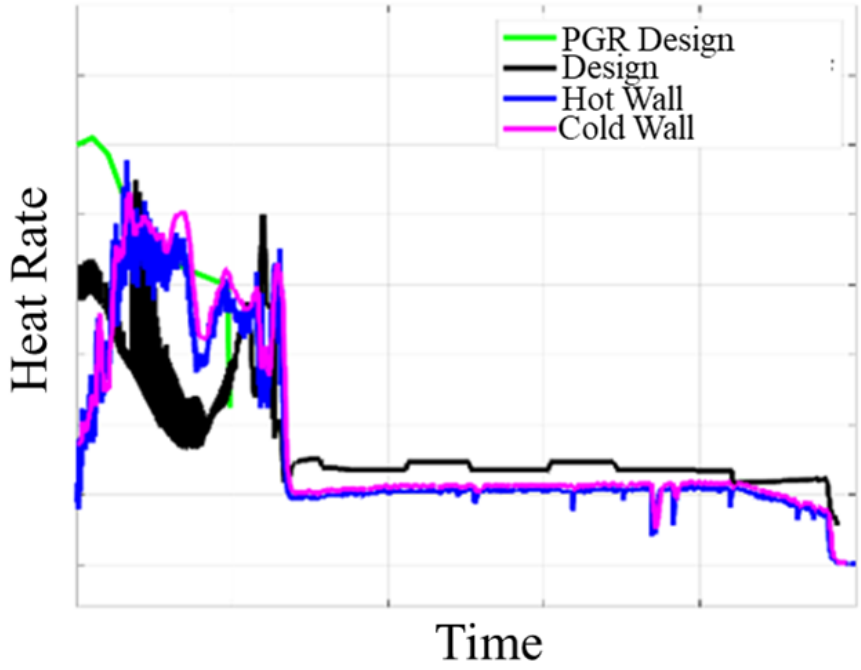


**Figure 21. Reconstructed total heat flux vs. time at the BHS off-center.**

*Solid Rocket Boosters*

The observation of the physics of the SRB plume to RS-25 plume interaction was a cardinal aerothermal objective, as this area was unique to the SLS vehicles as the SRB plumes were not near the RS-25 plumes in the Shuttle configuration. For this reason, a heavy cluster of instrumentation on the right SRB and left SRB was installed to substantiate the design environments resulting from the plume interactions.

The outboard five-segment SRB flight instrumentation in the base region was expected to be very similar to that of Shuttle-era four-segment SRB. Four and five-segment SRM ground test data showed similar type plume phenomena; it was expected the differences in environments would be more driven by the changes in motor positions (compared to Shuttle), five-segment chamber conditions, and altitude (plume expansion) trajectory characteristics. The flight data concluded that there was very little variation between Shuttle and SLS environments on the outboard regions of the SRBs.

The greatest disagreement between the predicted plume convection and flight occurred at the inboard region of the SRBs just aft of the CS BHS. From BHS and SRB DFI, it was confirmed that the additional energy release from BHS TPS combustion increased the overall convection

inboard of the SRB aft skirt. The induced convection from these biproducts was not predicted in the design environments. This period of flight was expected to reflect plume-induced aspiration as observed in Figure 22. Most of the P50 cork on the SRB aft skirts were on the forward components. PGR test data showed convective heating from the release of the chemical potential energy in the P50 cork pyrolysis gas products. However, while PGR design environment changes were made to the CS BHS, the additional heat release was not modeled at the SRB aft skirt.

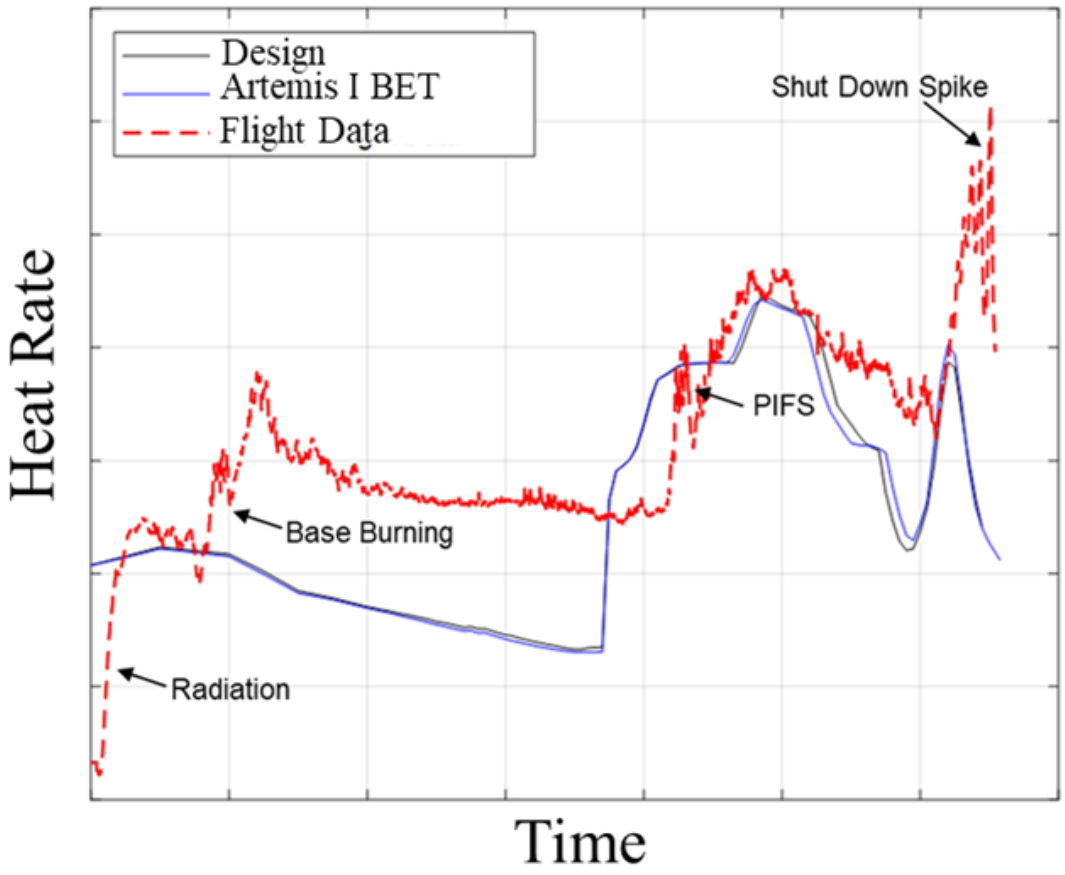


**Figure 22. Base burning was observed in SRB flight data.**

It is critical to note that specifically the SRB aft skirt gauges, while they are forward of the SRB base, are still within the recirculated region of the CS base gas. The SRB nozzles act to plug-up the CS vent areas between RS-25 engines and when the RS-25 and SRB plume interactions begin, the inboard aft skirt areas are heated with the CS BHS. While typically DFI forward of the SRB base would be utilized to capture Plume-Induced Flow Separation (PIFS) environments, these gauges are uniquely blocking the base vent areas; for this reason, it is important to make this distinction and the base heating implications for this portion of the SRB aft skirt. In other words, at this location, the flow field and SRB gauges do not reflect PIFS, but rather shows environments that are associated with SRB and RS-25 plume-induced recirculation. This is clearly shown in Figure 23 where the SRB aft skirt calorimeter response is in-synch with the CS calorimeter and CS GTP where base burning was observed.

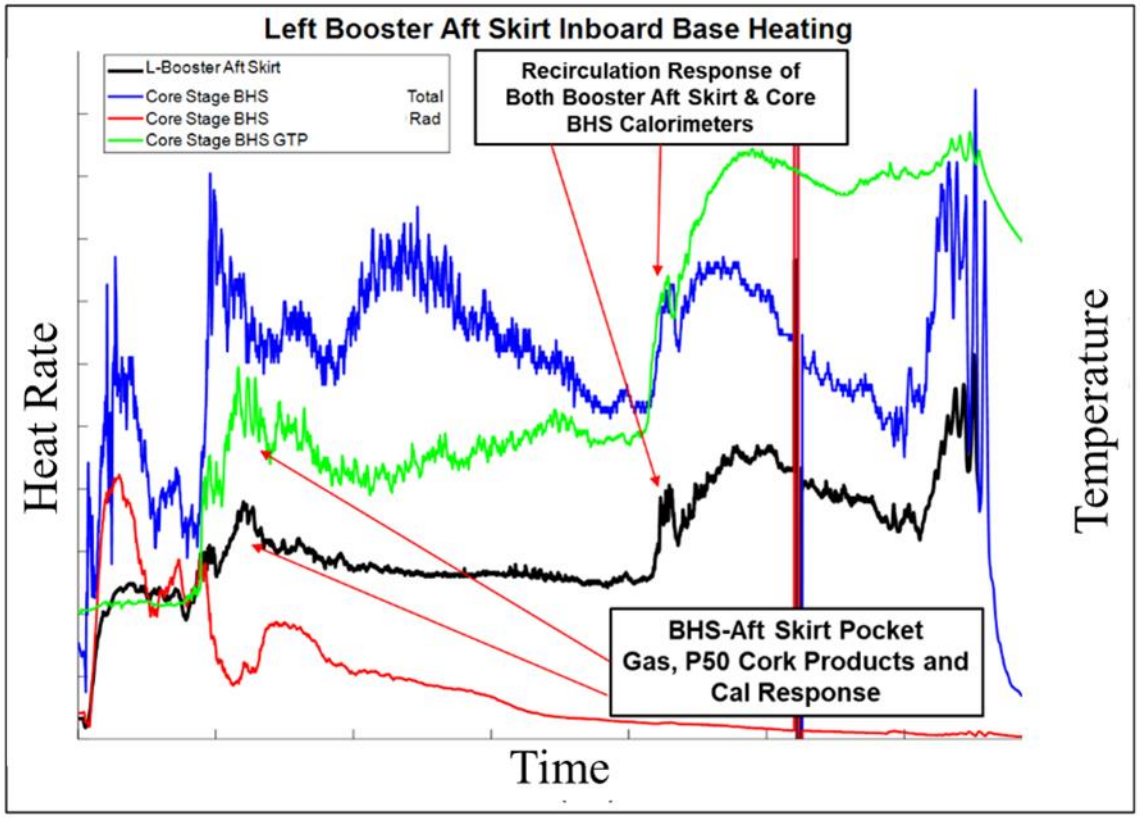


**Figure 23. SRB aft skirt calorimeter response in-synch with CS calorimeter.**

Body point models within the inboard SRB aft region were updated to incorporate the impacts from P50 cork burning products, in areas along the aft skirt, thermal curtain, and nozzle. These updates will act to prevent body point peak heat rate or total heat load exceedances for all future SLS flights.

Plume-Induced Flow Separation

Several instrumentation islands were mounted on the left SRB, CS engine compartment and LH2 tank to observe PIFS environments. These gauges were suited to capture the time and spatial distribution of the forward freestream separation point induced by the plume and to capture the pressure and heating characteristics of the recirculated gas in the separation zone.

Early in the SLS program, PIFS models were generated using a semi-empirical approach that utilized existing semi-empirical ground and flight test data to determine zonal environments throughout the SRB and CS. Given the four and five-segment SRB geometry similarities in the base region, it was determined that four-segment Shuttle data could be scaled for the use in SLS five-segment SRB plume-induced environment models. Predictions using CFD and wind tunnel testing were also performed, which provided a more composite picture of vehicle-booster plume separation phenomena. Given the uncertainties and the observed levels of conservatism between CFD, wind tunnel test data, and the semi-empirical flight data derived approaches, it was decided

to keep the Shuttle SRB PIFS models and semi-empirical CS environments. Generally, observations from the comparisons have shown the PIFS environment models to be conservative, with exception near areas where P50 cork burning induced environments made an impact to the local flow field.

*Core Stage*

CS PIFS design environments were shown to be conservative with respect to flight. Design environment models in the vicinity of the base, the boat tail, and engine shrouds, were based upon the 2% scale model wind tunnel test data. Furthermore, additional CFD was performed to model the PIFS to compare with semi-empirical models. Far forward of the BHS, within the engine compartment, models were based upon semi-empirical models developed from scale model and legacy flight data. Over predictions were driven by variation of the design trajectory and that of the BET trajectory, and the use of a zonal, bounding semi-empirical design environment approach that used bounding correlations (from scaled data) as opposed to individual design environment models developed from CFD. While use of semi-empirical zonal approach was shown to be conservative, it was based upon existing flight data and scale model wind tunnel ground test data and was relatively easy to implement. Comparisons of CS PIFS flight environments are shown in Figure 24.

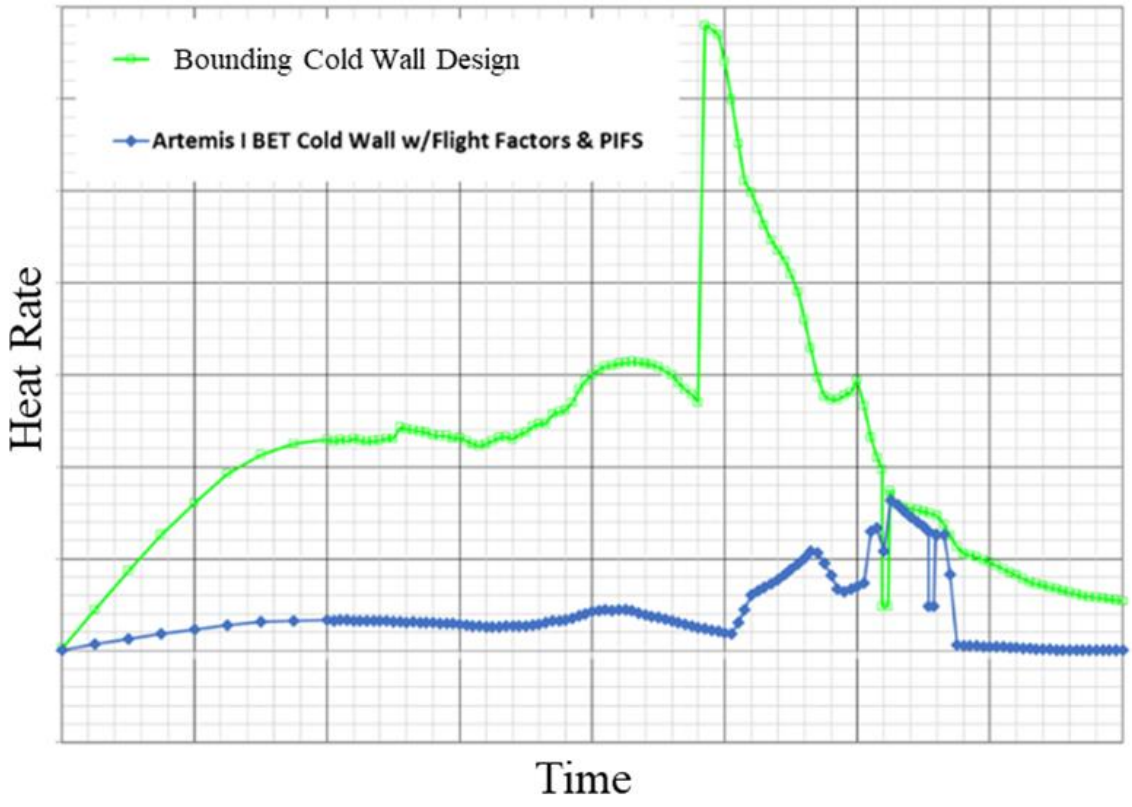


**Figure 24. CS PIFS generated based off flight data.**

*Solid Rocket Booster*

All design environments within PIFS regions were found to be conservative. Minor exceedances occurred at the inboard SRB aft skirt due to P50 cork burning-induced convection as previously discussed. While the aft skirt was forward of the SRB base, it was determined these exceedances were due to the burning of local BHS pyrolysis gases and were not assumed to be PIFS environments, review Figure 22. In all other areas, the PIFS environments at the SRB were shown to be less than the design models, attributed to the conservative assumptions within the PIFS prediction methodology. The design methodology utilized a zonal approach whereby the bounding environment was predicted to cover the vastness of geometries in the region. Examples of SRB PIFS environments are shown in Figure 25 and Figure 26.

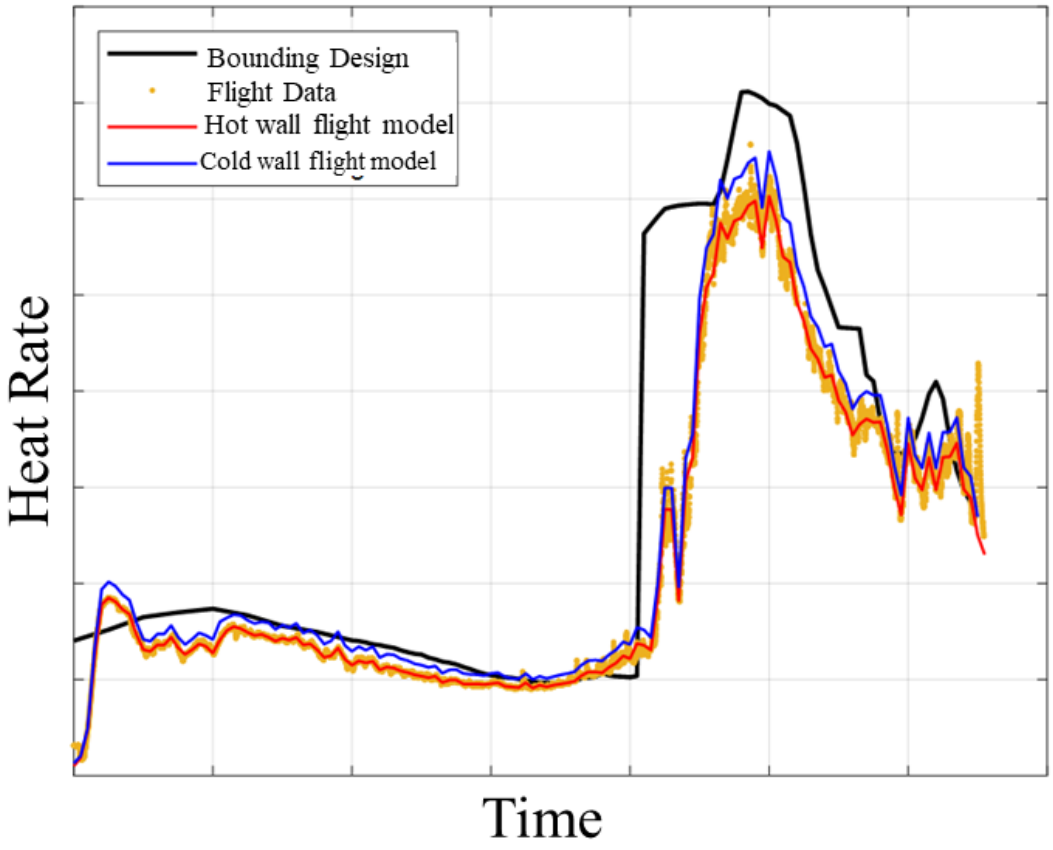


**Figure 25. PIFS observed on the SRB aft skirt kick ring.**

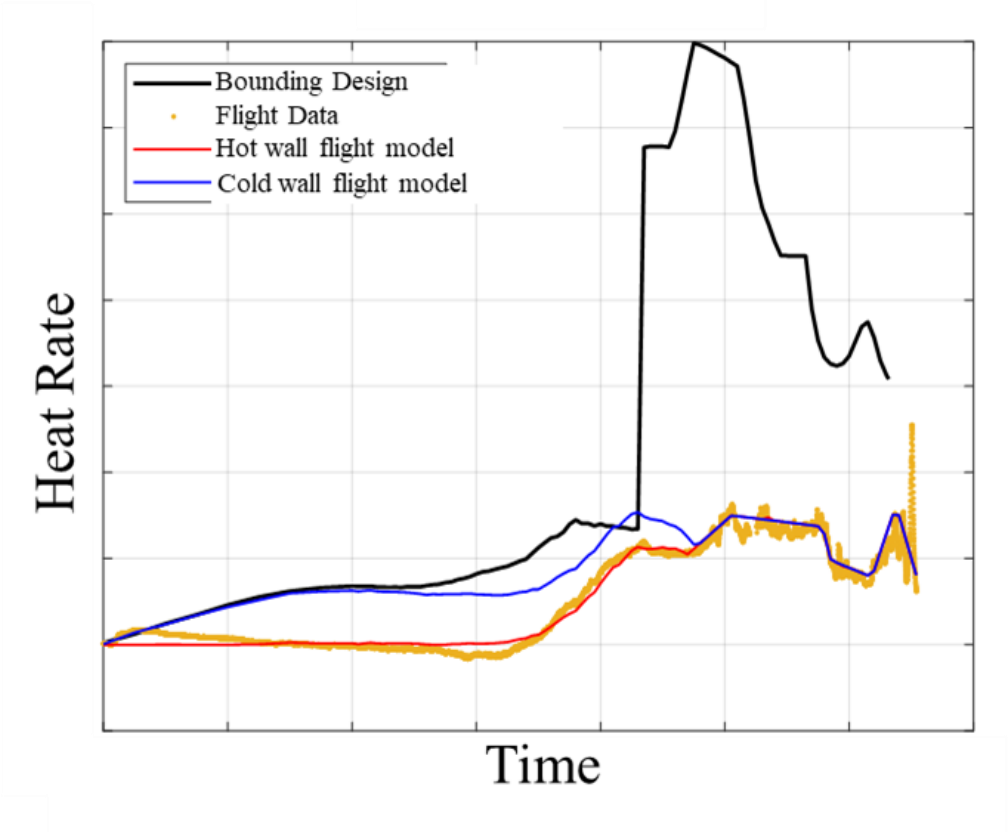


**Figure 26. PIFS observed on the SRB aft attach ring.**

One lesson learned regarding PIFS environments was its diminishment at higher altitudes as the launch vehicle left the atmosphere. One question that was looked to be answered with flight data was whether PIFS would extend forward of the CS after SRB separation. In investigating all the aspects of the flight data, it was concluded that with the decrease in density after SRB separation, PIFS environments became so low that they were indistinguishable from that of other heat sources (sun, earth albedo) and out of the range of the calorimeters. Rarefied and free molecular heating levels were similarly nearly immeasurable, and the signal-to-noise ratio became very low. For these reasons, there appeared to be a minimum environment heat flux that could be reported with the installed instrumentation and environment uncertainty levels.

Plume Impingement

Several islands were mounted on CS forward skirt, LO2 tank, and LH2 tank to measure both the direct forward BSM plume impingement environments (environment within the core “inviscid” plume flow impingement), and the plume-induced environments that were a consequence due to the plume-freestream interaction (upstream plume-induced flow field separation, plume deflection, and downstream “hot wake” flow), and the plume-plume interactions (BSM plumes impinging on one another, resulting in a merged jet that furthermore impinges on the vehicle). Similarly, gauges were placed on RS-25 engines and engine section to measure direct aft BSM plume impingement environments and plume-induced aerodynamic phenomena.

Calorimeters, pressure transducers, and thermocouples were installed on the Orion MPCV LAS motor, fillet, and ogive areas to measure LAS JM plume impingement. Furthermore, thermocouples were installed throughout the Orion CM to provide the thermal responses with respect to the LAS JM plume impingement.

Flight imagery taken during the SRB separation and LAS jettison events were recorded under the backdrop of night, resulting in varying quality. Given the night launch, most parts of the vehicle were in darkness, and some of the views of the direct plume impingement were unfortunately obscured affecting the camera prior to BSM ignition. The brightness of the plumes further reflected off the debris clouds resulting in further obscuration of the view. TPS charring contours have been beneficial towards the validation of plume impingement heating distributions, as previously witnessed from BSM impingement on the Shuttle External Tank. Unfortunately, also due to darkness, visibility of the plume impingement TPS char contours on the CS tanks was not possible. LAS JM plumes were visible from the Orion forward hatch window; however, details of the impingement phenomena were not visible from other flight or ground cameras. Brighter areas of the plume are most likely a result of the radiative qualities of the plume particulates in the plume cores, in these cases zirconium-oxide (LAS JM) and aluminum-oxide (BSM).

### *Booster Separation Motor Plume Impingement*

Due to the highly transient characteristics of the BSM chamber pressure history and SRB dynamics, the plume development and plume-induced environments are changed at smaller time scales than that of the calorimeter response time and sample rate. As previously discussed, the on-board Data Acquisition System sampled the calorimeter measurements with a signal conditioning card that induced some data filtering that caused problems in the raw calorimeter and radiometer heat flux data affecting the reconstruction of the induced peak heat rate and load.

BSM plume impingement design environments throughout the vehicle were found to be generally conservative. At areas on the vehicle believed to be engulfed by the plumes, the predicted environment magnitudes were generally higher than what was measured, in some places a factor of 5-10 times the measurement. It is believed this is partially due to the differences in plume impingement environment spatial distribution unique to the flight trajectory and flight motor conditions in comparison to that used in design. An example of BSM plume impingement design environments with flight data comparisons are shown in Figure 27. All predicted BSM impingement peak heat rates enveloped the measured flight responses.

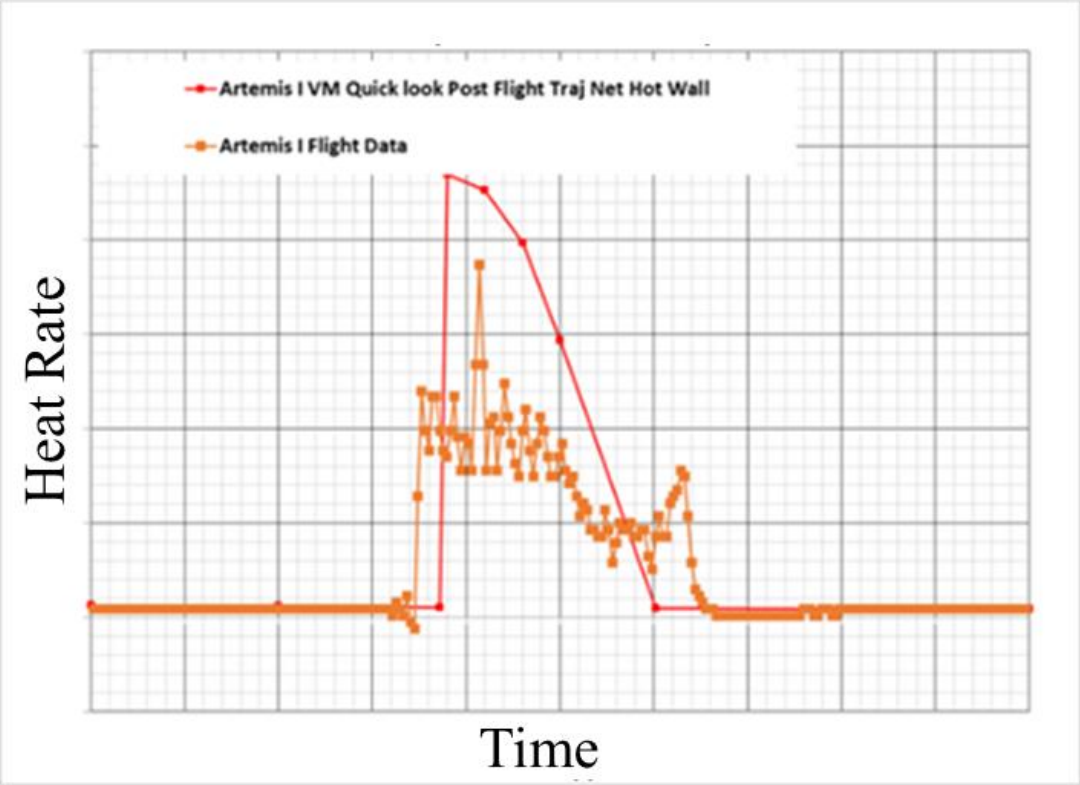


**Figure 27. CS BSM model envelopes flight data.**

The aft BSM plumes impinged on the aft portion of CS including two of the RS-25 engine nozzles. Based upon the gauge responses and CFD results at the flight conditions, it was observed that the aft BSM impingement on the RS-25 engines showed significant difference in heating contours than the environments used in design. The aft BSM impingement location and magnitude varied from the design environments due to the contrast in staging freestream conditions (lower dynamic pressure than design). An example of aft BSM plume impingement design environments with flight data comparisons are shown in Figure 28. BSM plume impingement design environments were developed early in the SLS Block 1 program (2014). CFD modelling was performed using max motor chamber conditions, a design trajectory and a MUF to determine CS and RS-25 impingement design environments. The flight data showed that the peak heat flux values were lower than those used in the design environments. While the design environments proved to be bounding for Artemis I, future consideration will be the use of a CFD database over the range of booster separation conditions to determine plume impingement environments in a Monte Carlo fashion.

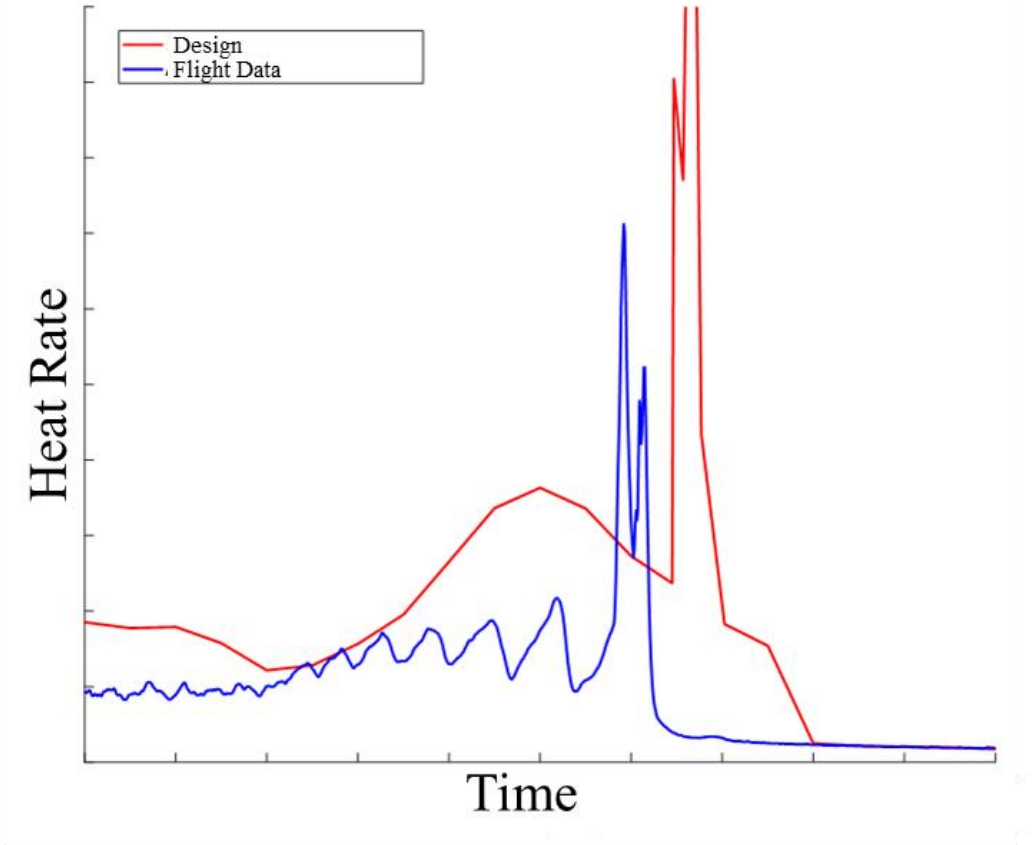


**Figure 28. Aft BSM impinged on the CS engine nozzle.**

One noteworthy difference between the BSM plume-induced design environments and flight was regarding the forward-most point of BSM plume-induced flow separation. The design environments predicted that the forward most point of BSM plume impingement was approximately at the Orion CMA Ring, just aft of the LAS ogive. Instrumentation on the LAS observed changes in pressure and heat flux indicated that the BSM plume impingement occurred up to the LAS nose. Imagery captured by MARS cameras showed the BSM plume-plume interactions generated a reflected shock upon the merging of the jets; the merged jet penetrated the freestream crossflow deeper than that of a single BSM plume, see Figure 29. While this phenomenon was modeled in pre-flight CFD simulations, the BSM nozzle exit jet pressure ratio at flight conditions was higher than pre-flight design. In penetrating deeper in the cross flow, the merged jet separated the flow. The flow separation induced by the BSM plume results in a forward shock that sweeps the vehicle up to the nose. The post shock heat flux pulse is shown in Figure 30.

While the forward shock heating from the BSM impingement was not accounted for in the design models for Orion MPCV, generally the relative heat flux magnitudes and integrated heat load of the pulse was accommodated by the conservative aerodynamic heating models. Post flight BSM plume impingement environment models have been implemented all the way up to the LAS nose.

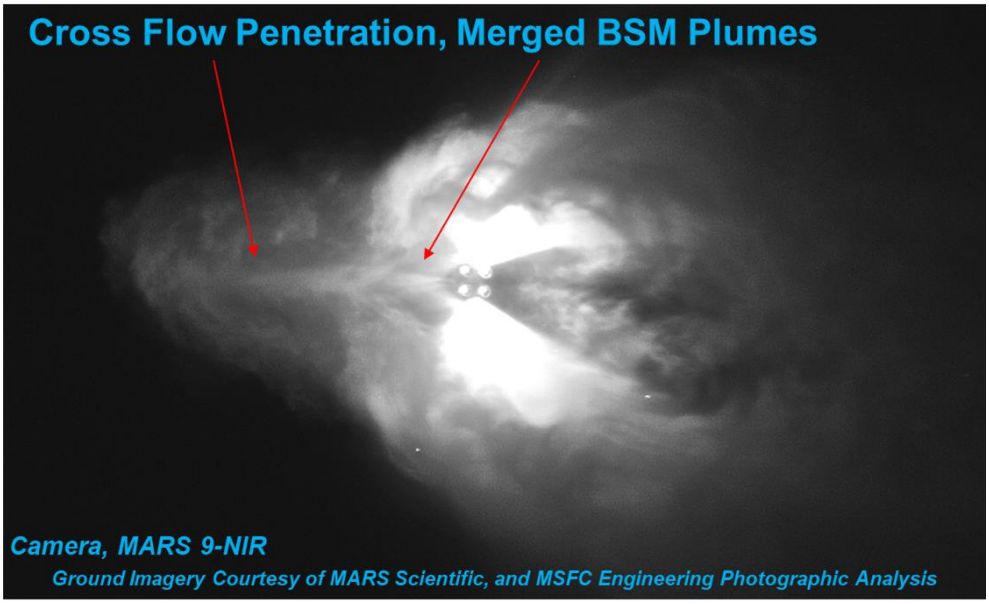


**Figure 29. Imagery captured the crossflow penetration from the BSM Impingement.**

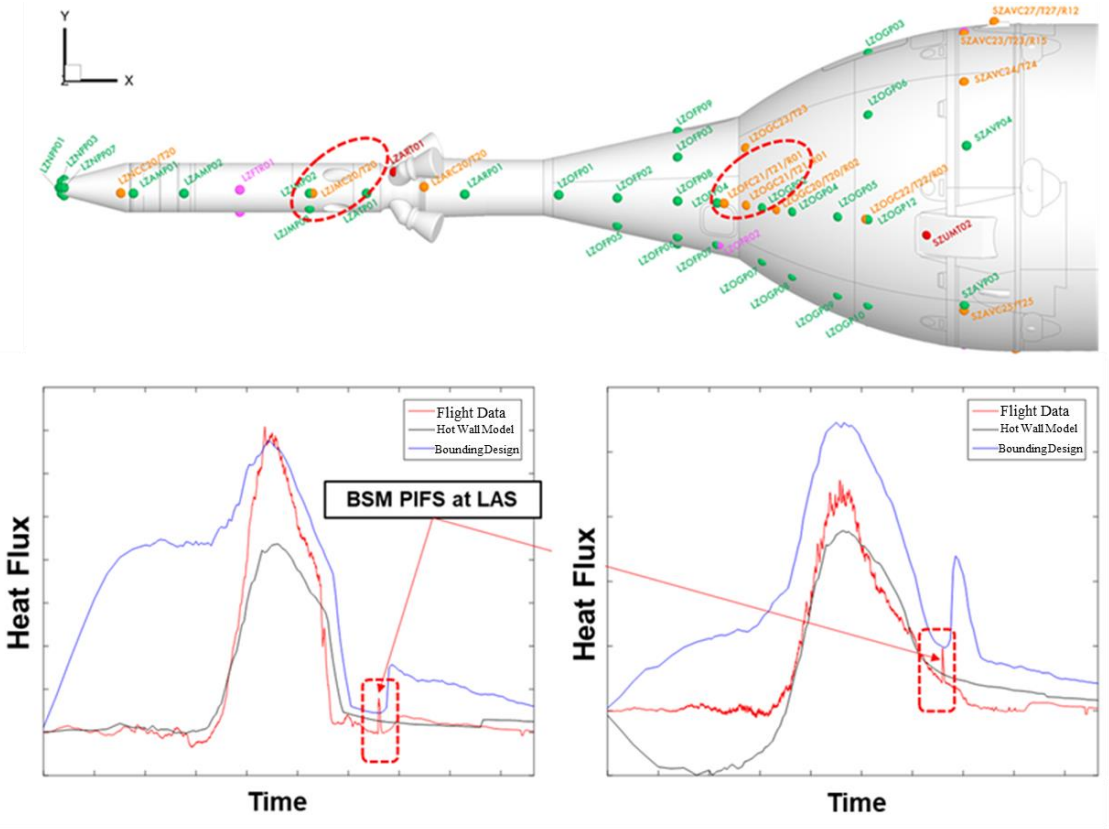


**Figure 30. BSM spike shows up on all gauges on the MPCV.**

*LAS Jettison Motor Plume Impingement*

LAS JM plume impingement design environments were developed back in 2009 under the development of Orion under the Constellation program. Environments were measured by Orion MPCV DFI and were impacted by data filtering; the peaks were presumed to be clipped. An example of LAS JM plume impingement captured from Orion MPCV DFI is shown in Figure 31. Overall the predicted LAS JM environments were found to be conservative and bounded all flight data.

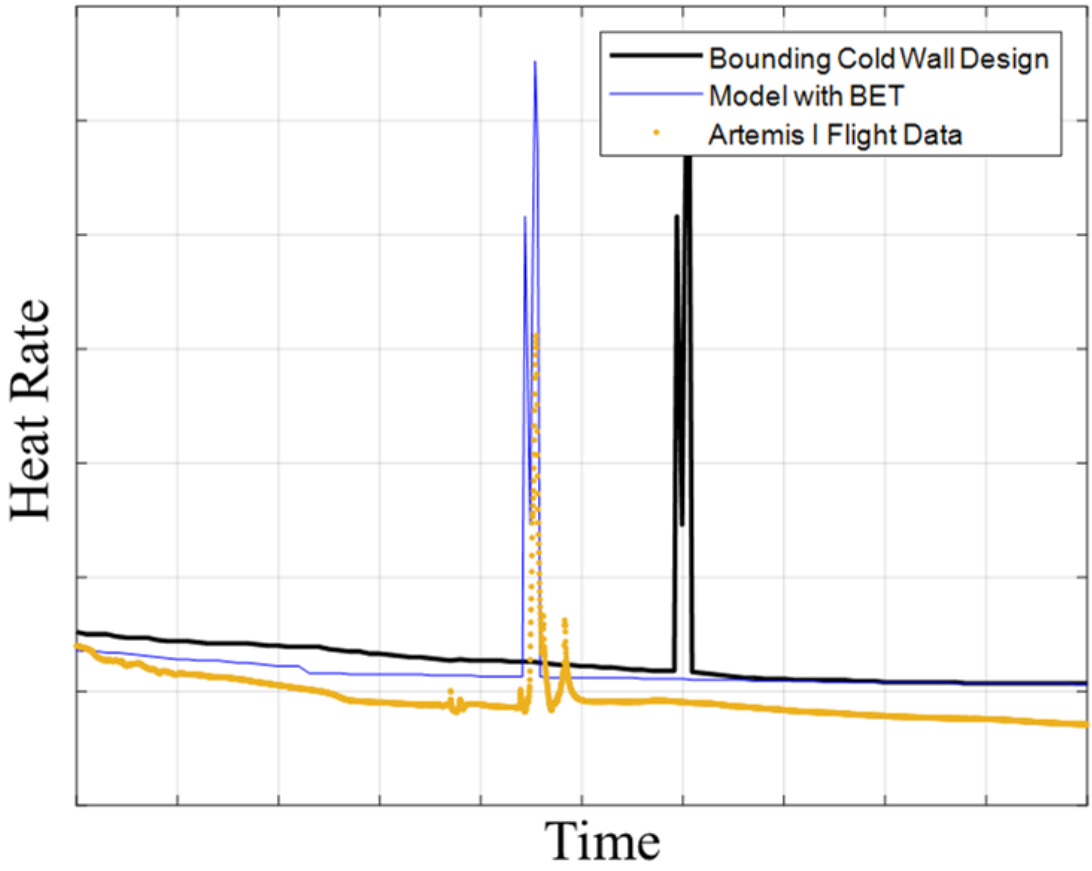


**Figure 31. LAS Separation plume impingement was observed on MPCV DFI.**

Ascent design environments were developed for the Orion CM and SM following SAJ panel separation and LAS jettison when they become exposed to the freestream. The CM and SM are initially exposed to the LAS separation plume as it sweeps across and away from the vehicle. Onboard cameras captured the LAS Jettison as seen from the CM, see Figure 32. This environment was also seen in the temperature gauges on the CM. Figure 33 shows an example of the heat flux estimated from the temperature gauge compared to the design environment. Again, it was believed that any filtering of flight data clipped the peak heat flux and reported a lower magnitude.

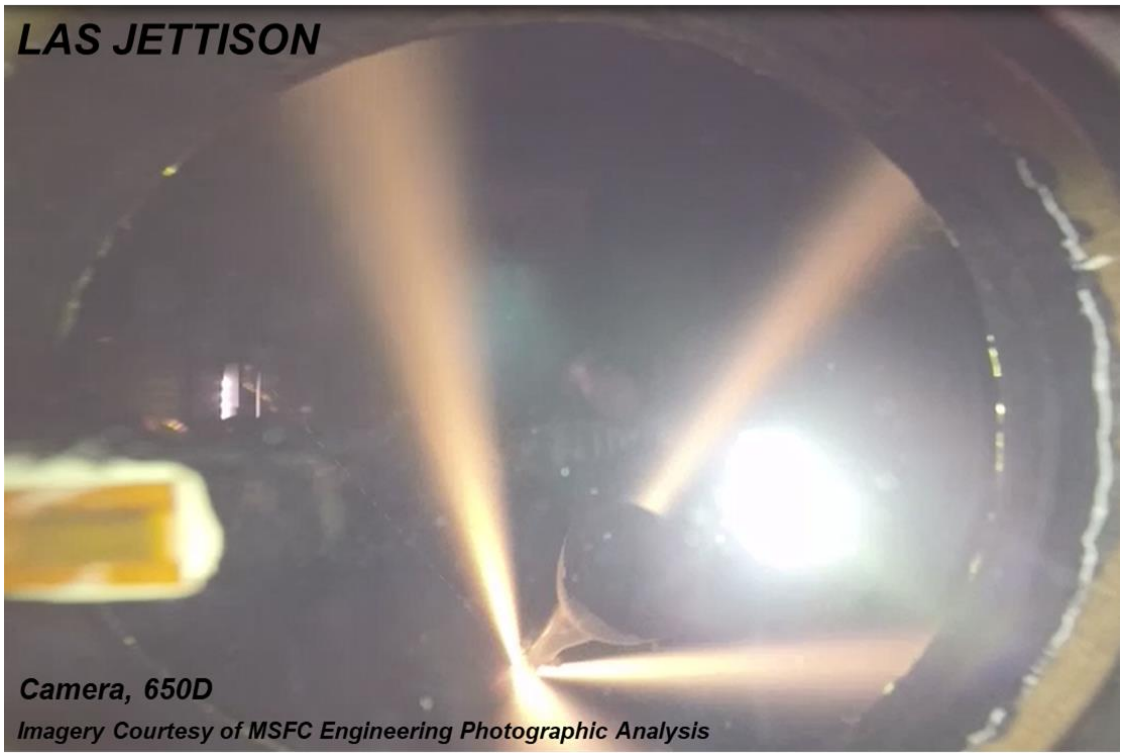


**Figure 32. LAS jettison motor plumes as viewed from the Orion window.**

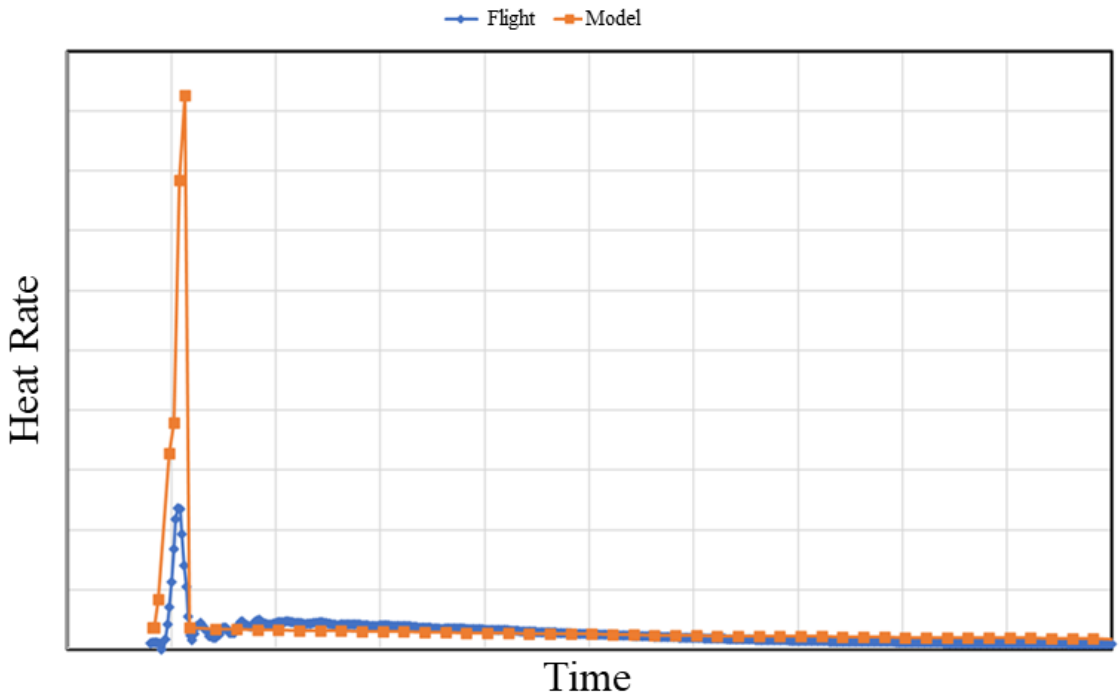


**Figure 33. MPCV environments underneath the LAS are exposed to LAS separation plume impingement.**

CAPU Plume Heating

There were a total of four Core Auxiliary Power Units (CAPU) that provided power for valves and hydraulic gimballing of the 4 RS-25 engines for vehicle control authority. Two pairs of ports were on the venting region of the BHS away from the SRBs. Each CAPU operated at two hydrogen mass flow states: a high flow rate, high exit pressure and a low flow rate, low exit pressure. During the CAPU high-flow state, the CAPU exhaust plume can impinge on the RS-25 nozzles. During the low-flow state, the CAPU exhaust plumes were very close to the BHS and sometimes attached to the local surface of the heat shield near the port exit. Following engine start-up, the CAPU free hydrogen exhaust plumes lift-off the surface (diffusion flame) and the local flow attachment and impingement lead to considerable convective heating on the BHS.

During prelaunch, while the vehicle was stationary on the pad, the CAPU exhaust disposal impacted on the base flow field as evidenced in the base heat shield gauge responses. Measured flow rates were synched with calorimeter data, Figure 34 shows data over the period of RS-25 start up to SRB ignition. Without SRB radiation to saturate the total heat source to the base, prelaunch data was ideal to isolate CAPU effects. Figure 34 is an example of prelaunch data on the BHS where CAPU plume heating is clearly evident. During start-up, the CAPUs operated using pressurized helium, once CAPU transitioned to hydrogen, a substantial increase in convective heating was observed. Heating oscillations are observed from the pulses generated from high-flow rate CAPU mode.

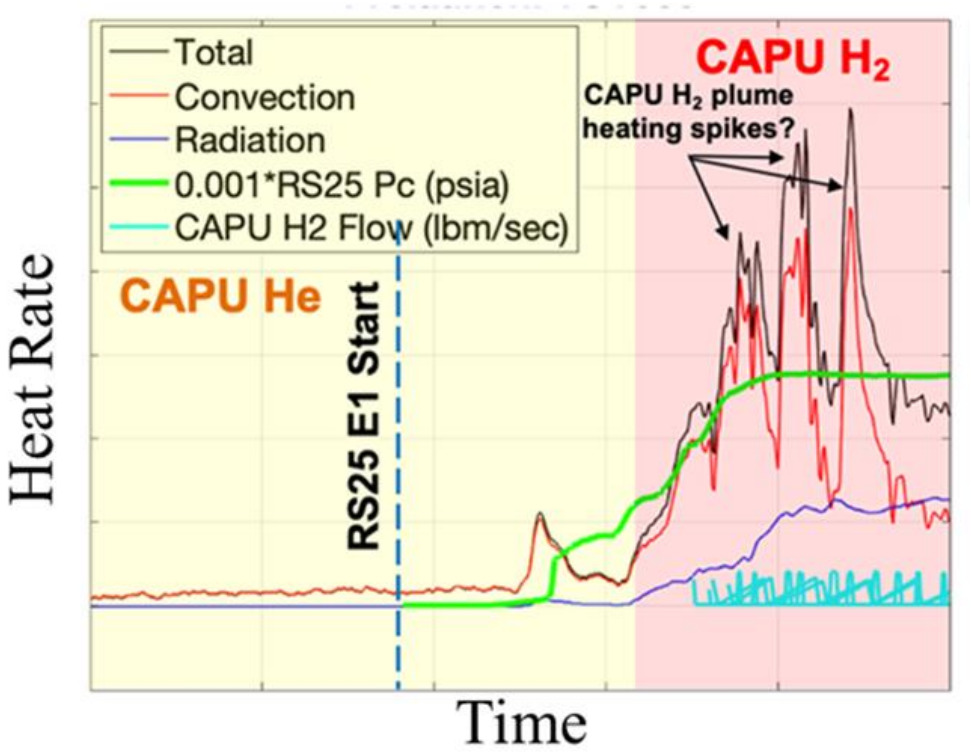


**Figure 34. CAPU was only prevalent in prelaunch data.**

The CAPU plume-induced heating and radiation from the RS-25 plume Mach discs were the greatest sources of heat flux, both included in the prelaunch aerothermal models. Following lift-off the calorimeter responses no longer reflected the variation in CAPU mass flow rates, but rather measured the convection from the recirculated base flow mixture, following H2-burning that was injected base volume. Post flight the prelaunch aerothermal environments were revised to reduce conservatism. Furthermore, during the plume-induced aspiration phase of flight, base convection models were revised to predict convection from the base mixture of entrained air and combusted hydrogen (recirculated in the base) as opposed to models from discrete plume impingement environments from varying CAPU mass flow rates.

## CONCLUSION

The main conclusion was that the Artemis I SLS vehicle had a nominal flight related to aerothermal environments and no anomalies were observed. Several updates to the models were implemented to improve overall modeling accuracy.

The comparisons reveal the fidelity of the design models, highlighting areas where the design models accurately predicted flight conditions and instances where deviations were observed. Preliminary results suggest that while the design models largely aligned with the observed flight data, there were unique observations that reflected needed areas of model refinement. Aerothermal flight data from Artemis I for the SLS Block 1 vehicle will be further utilized to enhance the accuracy of Block 1B and Block 2 aerothermal models, ensuring improved safety and performance for subsequent Artemis missions.

## ACKNOWLEDGEMENTS

This document presents the SLS external thermal design environments based on analysis performed by the NASA Marshall Space Flight Center Aerosciences Branch in support of the SLS Program. This document was produced through the efforts of many individuals with significant contributions coming from: Craig Schmitz, Chrissi Papworth, Charles “Irv” Stuckey, David Brewer, Tyler Ekaitis, Francisco Canabal, Josh Wilson, Manish Mehta, and Sheldon “Bud” Smith under the supervision of the Branch Chief, Christopher Morris, and Aerothermodynamics Team Lead, Brandon Mobley.

## REFERENCES

1. Engel, C. D., Praharaj, S. C., and Schmitz, C. P., “MINIVER II Upgrade for the AVID System, Volumes I&II”, Remtech Report RTR 123, February 1988.

2. NASA, “NASA’s Space Launch System: Reference Guide”, Version 2, released August 2022.

3. Westkaemper, J.C., “On the Error in Plug-Type Calorimeters Caused by Surface-Temperature Mismatch”, Journal of the Aerospace Sciences, Volume 28 Issue 11, Nov. 1961.

4. Morris, C.I. (2015), "Space Launch System Ascent Aerothermal Environments Methodology", 53rd AIAA Aerospace Sciences Meeting, AIAA SciTech, (AIAA 2015-0561), Kissimmee, FL.

5. Svehla, R.A., and B.J. McBride, "FORTRAN IV Computer Program for Calculation of Thermodynamics and Transport Properties of Complex Chemical Systems," NASA TN D 7056, January 1976.

6. Smith, S.D., "High Altitude Supersonic Flow of Chemically Reacting Gas Particle Mixtures Volume I, A Theoretical Analysis and Development of the Numerical Solution," LMSC HREC TR D867400 I, Lockheed Missiles & Space Company, Huntsville, Ala., October 1984.

7. Taylor, M.W. and H.S. Pergament, “Standardized Plume Flowfield Model SPF II, Version 5, Volume II – Program User’s Manual, PST TR-60-II, Propulsion Sciences and Technology, Langhorne, PA, September 2005.

8. Reardon, J. E. and Lee, Y. C., “A computer Program for Thermal Radiation from Gaseous Rocket Exhaust Plumes,” REMTECH RTR 014-9, December 1979.

9. Everson, J. and Nelson, H.F., "Development and Application of a Reverse Monte Carlo Radiative Transfer Code for Rocket Plume Base Heating," Journal of Thermophysics and Heat Transfer, 7 - 4, (1993)

10. Mehta, M., Mobley, B., Smith, S.D. (2024), “Space Launch System Base Aerothermodynamics Post-Flight Reconstruction for Artemis I”, AIAA SCITECH 2024 Forum, (AIAA 2024-0256), Kissimmee, FL.